Filamentary Hα structure in the milky way

Andrew J. Walker
University of Wollongong

FILAMENTARY Hα STRUCTURE IN THE MILKY WAY

A thesis submitted in fulfilment of the
requirements for the award of the degree

DOCTOR OF PHILOSOPHY

from

THE UNIVERSITY OF WOLLONGONG

by

ANDREW J. WALKER

Department of Engineering Physics

2006

Abstract

The first part of this thesis presents the first results of a search for new optical supernova remnant candidates and other filamentary objects on films produced by the Anglo-Australian Observatory/UK Schmidt Telescope Hα Survey. Sixty-one fields, or 26 percent of the Galactic plane survey fields, have been visually examined. This resulted in the detection of four new large diameter filamentary structures, and the discovery of extensive new optical emission in two previously known optical supernova remnant candidates.

The second part of this thesis presents results of a study we made using the FLAIR instrument on the UK Schmidt Telescope to obtain optical spectra of several filaments in RCW 114, a filamentary nebulae of about 250 arcmin diameter. These confirm that the emission is being produced by the interaction of the shock wave of a supernova remnant with the surrounding interstellar medium. We also obtained narrow-band Hα+[N II] and [S II] images to examine the spatial variation in ionisation structure.

The third part of this thesis gives the result of a search using films from the UKST Hα Survey where the locations of 86 Galactic supernova remnants were examined for optical emission. From these we had likely detections of 8 objects and possible detections of 4 others. We have discovered a new loop of emission nebulosity, 10° in diameter, which we have named the Coalsack Loop.

Acknowledgements

Firstly thanks must go to my supervisor Bill Zealey, who first encouraged my interest in Astronomy as a work experience student and then got me interested in supernova remnants for my Honours project. Throughout the years he has provided much valuable advice in all areas of astronomy and help keep me focussed along the long road to the completion of this thesis.

I'd also like to thanks the many staff I have been involved with at the University of Wollongong during my time as a student, who may have at some stage been my lecturer or provided other forms of help: Peter Anthony, Peter Fisher, Carey Freeth, Peter Ihnat, Michael Lerch, Roger Lewis, David Martin, Jagdish Mathur, Glen Moore, Paul Nulsen, Anatoly Rozenfeld, Phil Simmonds, George Takacs, Rodney Vickers and Chao Zhang.

Thanks must also go to the many other students at the University of Wollongong who have provided assistance over the years with observing, data reduction, general computer usage and many other areas. These include fellow astronomy students Stacy Mader, Vincent McIntyre and Erik Muller, along with Richard Baker, Duncan Fisher and other fellow lab demonstrators.

Special thanks also must go to the staff at the UK Schmidt Telescope, Quentin Parker, Fred Watson, Paul Cass, Malcolm Hartley and Ken Russell who provided great assistance during my observing runs and also my stay during 1998. I also thank the staff at the AAT and AAT lodge. In addition thanks goes to Mike Bessell, Anne Green, Brian Gaensler and Miller Goss who have all provided assistance and advice, and the anonymous referees who have provided feedback on my papers.

Finally I'd like to thank my family who have shown patience and given support through the years, and help me fulfill my ambitions of completing this work.

Publications

- Chapter 2: Walker, A.J., Zealey, W.J. & Parker, Q.A., 2001, **Filamentary Shell Structures from the AAO/UKST Hα Survey**, PASA, 18, 259
- Chapter 3: Walker, A.J. & Zealey, W.J., 2001, **Multifibre Spectroscopy of the Supernova Remnant Candidiate RCW 114**, MNRAS, 325, 287
- Walker, A.J. & Zealey, W.J., 1998, **Searching For Supernova Remnants**, PASA, 15, 79

Certification

I certify that the work presented in this thesis is my own, except where stated and or referenced as otherwise.

Andrew Walker

July 2006

Contents

List of Figures

List of Tables

Chapter 1

Supernovae, Their Remnants, and Wind-Blown Shells

1.1 Supernovae

Historically, the classification of supernovae has been made on the basis of optical spectroscopy and light curves. Type I and Type II are separated by the presence of hydrogen in their spectra, the former having none. Further subdivision within these classes is made on the basis of other lines and in some cases the shape of the light curve. The main problem with this classification is that all but the Type Ia SNe are produced by core collapse.

1.1.1 Type I Supernovae

Sn Ia

These supernovae have Si II absorption at 6150 Å which is absent in types Ib and Ic. A further distinction is that after several months, Sn Ia spectra are dominated by blends of Fe emission lines, whereas types Ib and Ic have unblended emission lines of elements such as O and Ca. The progenitor is a white dwarf in a binary system which is accreting mass from the other star. When the white dwarf's mass reaches the Chandrasekhar limit of ∼1.4 solar masses, it is destroyed by thermonuclear detonation. The resulting explosion has an energy of $\sim 10^{51}$ ergs and an absolute magnitude of ∼-19.5.

SNe Ia have also been proposed as distance indicators for use in cos-

mology. This is through the assumption that they all have an identical peak luminosity once it is normalised by the light curve shape.

Sn Ib and Ic

Types Ib and Ic have more in common with Type II SNe than type Ia. They are formed by massive stars which have lost their hydrogen envelope, and in the case of Type Ic the helium envelope as well. This loss is due to stellar winds (e.g. Wolf-Rayet stars) or mass loss to a binary companion. The presence of moderate strength optical He I lines (e.g. at 5876 Å) distinguishes Ib from Ic. Their light curve shape is also similar to Type Ia, however the late exponential decline is at a slower rate. It has recently been suggested that Type Ib and Ic SNe may be associated with some gamma-ray bursts (Stanek et al. 2003).

Type II Supernovae

Type II SNe result from the core collapse of massive stars (greater than about 8 solar masses), and have hydrogen lines in their spectra near maximum brightness. They are less luminous than Type I SNe, reaching an absolute magnitude of $\sim$-18. Both the spectra and light curve, however, show more variation than Type I SNe. The Type IIb objects have a spectra dominated by He at $\sim$3 months, whereas Type IIL and IIP objects' spectra are still dominated by H. These last two are distinguished by the shape of their light curve after maximum, being linear or having a plateau respectively.

Other types have been proposed, including IIN SNe. Their spectra have strong but narrow emission lines, chiefly Hα, on a base of FWHM 1000-2000 km s^{-1}, or even larger. In these there is a strong interaction between the ejecta and dense circumstellar gas.

Sn IIb

These SNe show a transition from the hydrogen-rich type II spectra to that more resembling a Type I devoid of hydrogen later in their life. Two of these, SN 1993J (reviewed in Filippenko & Matheson 2005), and SN 2001ig (Ryder et al. 2006) have had a companion star directly detected. It is believed

that the companion star strips hydrogen from the primary, leaving it with a thin hydrogen shell.

Sn IIL and IIP

Type IIP show a plateau region in their light curve from 50-100 days, typically a magnitude below peak brightness. This is absent in Type IIL which decline steeply after maximum. Both result from the core collapse of a massive star with a outer hydrogen shell. This is of a few solar masses in Type IIL up to ten solar masses for Type IIP. The SN 1987A, in the Large Magellanic Cloud, was classified as Type IIP.

1.2 Supernova Remnant Evolution

The shock wave of a supernova initially expands supersonically into the surrounding medium. Its subsequent evolution will depend on the interaction of this remnant with the surrounding gases, initially this material may have been influenced by wind and radiation from the star. In the later stages, the properties of a remnant will depend mostly on the properties of the interstellar medium.

To simplify matters, the earliest models of an expanding remnant made the assumptions that:

- The expansion is into a homogenous intercloud medium
- The ejecta of the star's outer layers expands outwards as a uniform spherical shell.

This allows the evolution to be generalized into four stages, which can be described by self-similar solutions (Woltjer 1972, Gull 1973, Chevalier 1977, Reynolds 1988)

1.2.1 Free Expansion

Initially the shell of ejected material will expand outwards at a constant velocity. In front of this is a small mass of swept up material. A reverse shock propagates back into the ejecta, heating it. After a few hundred years the swept up gas will have a mass similar to that of the ejecta.

1.2.2 Sedov-Taylor (Adiabatic) Expansion

In this stage the mass of gas swept up is several times larger than the mass of ejecta, and the shock decelerates. The shock radius increases with time by $R_s \propto t^{2/5}$ and a velocity of $v_s \propto t^{-3/5}$. During this stage the radiative energy losses are negligible compared with the initial explosion energy.

1.2.3 Radiative (Snowplough) Phase

Further in the shock's evolution, the cooling time of gas which has passed through the shock is similar to the expansion age. Radiative losses become important. Cooling of the shell makes the energy radiation more efficient, increasing the rate of cooling. The expansion velocity rapidly decreases, now $R_s \propto t^{2/7}$ and $v_s \propto t^{-5/7}$. Expansion is driven by momentum, which is conserved. In this *snowplough* phase a cool, thin shell has formed.

1.2.4 Dissipative Phase

After a time of typically $1 - 2 \times 10^5$ years, the expansion velocity drops to below the local ISM sound velocity. The shell breaks up and the remnant becomes indistinguishable from the surrounding medium.

In reality the evolution of supernova remnants may differ dramatically from this model. The ISM is usually non-uniform, especially if it contains clouds of denser material. Some remnants also expand into a pre-existing bubble from the progenitor star, OB associations or other supernova explosions. This will result in stages being lengthened or dramatically reduced, and non-uniformity of the remnant. The shape of the remnant may also be influenced by strong magnetic fields within the ISM.

1.3 Supernova Remnant Types

In chapter 2 we discuss the optical morphology of SNR. However most remnants have not been seen optically but only by their radio emission. The commonest are shell-type remnants, where a ring structure is visible due to the dense material being gathered up by the expanding shock wave. This limb-brightening

is seen as synchrotron emission, electrons are accelerated to relativistic speeds by the passing shock and the local magnetic field.

Plerion or Crab-like remnants are strongly influenced by a central pulsar. They have less of a shell structure and have radio brightness increased at the centre with a flatter radio spectrum. Other objects may show a mixture of these morphologies. Thermal composites are shell-type in radio emission but crab-like in X-rays. Plerionic composites have shells and have a crab-like appearance in radio and in X-rays.

1.4 Optical Emission of Supernova Remnants

Downstream from the shock in a SNR, heated material will cool down through radiative processes. Once below ∼15000 K, optical emission will appear. Often this is dominated by the Hα and Hβ lines. Because the gas has been collisionally excited, however, forbidden line emission from species such as [O II] and [S II] will normally be present.

Many optical SNR have been studied spectroscopically to derive physical properties of the shock and the local medium. As discussed by Aller (1984), X-ray emission in the Cygnus Loop indicates a gas of T = 2×10^6 K, and a shock velocity of $300-400$ km s^{-1}, which would require $\sim 10^5$ years to cool sufficiently to produce the filaments' optical emission. This is much larger than the remnant's age of 5000 to 8000 years (Blair et al. 2005).

In most cases the SNR is expanding into a cloudy ISM. As the shock overtakes a cloud, a lower velocity shock will propagate into the cloud and become radiative. Typically the shock velocity in the cloud will be $v_c = 60 - 300$km s^{-1} and the initial cloud density under 100cm^{-3}. Sometimes denser molecular clouds will be swept up, with a slower shock, $10 < v_c < 25$km s^{-1} in the cloud, producing molecular lines in the infra-red (cloud shock data from Dopita, 2003).

The relative intensities of optical lines produced by collisionally excited gas is sensitive to the physical conditions of the shock and gas. For the important forbidden lines in SNR, the ions can be treated as a three level-system comprising of a ground state and two excited states.

If the three energy levels are approximately evenly spaced, the triplet of resulting lines will be a diagnostic of the plasma's electron temperature. An

example is the [O III] ion which produces a triple of lines at 4363Å, 5007Å, and 4959Å.

A second case is when the energy difference between the two excited levels is much less than the energy difference between these and the ground state. An example is the closely spaced [S II] lines at 6717Å and 6731Å, which are typically strong in SNR emission spectra. The ratio of these two is sensitive to the electron density in the plasma. By combining data from temperature and pressure ratios the temperature and density can be determined simultaneously. Further details of this can be found in references such as Dopita (2003) and Aller (1984)

Chapter 2

Filamentary Shell Structures from the AAO/UKST Hα Survey

This chapter is based on published material Walker et al., 1998, "Filamentary Shell Structures from the AAO/UKST Hα Survey", PASA, **18**, 259.

2.1 Introduction

Extensive radio surveys within our galaxy have led to the discovery of 225 supernova remnants as of August 2000 (Green 2000). Of these a small number, including the Crab and Vela remnants, optically present us with a beautiful and complex picture of how the shock wave of a supernova interacts with the surrounding interstellar medium. By examining closely the relationships between the emission seen in different wavelengths, we can obtain a good picture of the processes occurring within the remnant. Most SNRs have been detected through their radio emission; optical counterparts are hard to find because of extinction.

Hα emission from gas in our Galaxy provides us with a picture of how the interstellar medium is being influenced by stars. This gas may be excited in a number of ways, chiefly by the radiation from hot stars, or the passage of shock waves from supernova explosions or strong stellar winds. The nebulae observed in Hα emission have a wide variety of morphologies. The emission may be diffuse, as seen in the Rosette Nebula, or filamentary, as seen in the Vela SNR. Partial or full shell structures are also often seen. Filamentary shell structures, the focus of this work, may be produced by Wolf-Rayet stars, Of and O(f) stars, the central

stars of planetary nebulae, and by supernova explosions.

All known optical SNR, apart from the oxygen rich class (Weiler & Sramek, 1988), emit in the Hα line, as well as the [N II] 6548,6583 Å lines. These are produced in regions behind the shock front, due to post shock cooling of the excited gas. The Hα survey will cover these lines and is well suited for SNR searches.

The AAO/UKST Hα Survey (Parker et al. 1999) has the potential to reveal fainter filamentary emission at a higher resolution than previously possible in a wide-field survey. This will improve our knowledge and understanding of optical SNR and other filamentary structures such as Wolf-Rayet shells by increasing the number and variety available for further study. We have recently commenced two projects. The first, the subject of this paper, is to visually examine survey films to discover new objects classifiable as SNR candidates based on their optical morphology, along with other shell structures. The second is to examine fields of known radio SNRs for optical emission (Walker & Zealey 1998).

Previous SNR searches have concentrated on known objects identified in other wavebands. This work covers the entire Southern Galactic Plane out to $|b|=10^\circ$ for the first time optically. The use of Tech Pan film and the Hα interference filter allows the detection of finer and fainter detail than any previous large area search (Parker, Phillips & Morgan 1998).

In order to ensure completeness of any SNR survey, future optical and radio searches will need higher sensitivities, and will need to be responsive to a wide range of angular scales, from sub arcsecond to several tens of degrees. The Hα Survey goes some way to meeting these requirements for our local region out to 4-5 kpc. Optical detections combined with radio observations will provide a more detailed picture of the nature of these objects.

2.1.1 Wind-blown Shells and Planetary Nebulae

Two hundred and twenty-seven Wolf-Rayet stars are known within the galaxy (van der Hucht 2000). These hot, massive young stars have broad emission lines in their spectra from He I and He II, along with various lines from excited states of carbon, oxygen and nitrogen. Of and O(f) stars are massive O stars which also exhibit a range of broad and narrow emission lines. Both of

these types have strong stellar winds, typically $v_w = 10^3 - 4 \times 10^3$ km s^{-1} and $\dot{M} = 10^{-6} - 10^{-4}$ M$_\odot$ yr^{-1} (Lozinskaya 1992). The stellar wind interacts with the surrounding ISM, which will include matter previously ejected by the star. Optical ring structures resulting from this interaction have been observed around many of these stars. Details on searches around Wolf-Rayet stars can be found in Heckathorn, Bruchweiler & Gull (1982), Miller & Chu (1993), Marston, Chu & Garcia-Segura (1994a), Marston et al. (1994b) and Marston (1997), in which it is concluded that more than one-third of Galactic Wolf-Rayet stars are associated with nebulae. A study of nebulae associated with Of stars (Lozinskaya 1992 and references therein) discovered ring nebulae associated with 12 stars.

Driven by the stellar wind, these nebulae may expand to over 100 pc in size. Those observed in our galaxy are mainly between 5 and 20 pc in size (Chu 1992). Their angular diameters vary from a few arcminutes to a few degrees.

Planetary nebulae may also exhibit filamentary structure. Some of their main properties of relevance here are widely varied morphologies; spectra similar to H II regions; hot, low mass central stars, mainly early O-type stars, Of stars and Wolf-Rayet stars; and a size of $\sim$0.8 pc (Kaler 1985;Kitchin 1987). Their progenitors are normally evolved asymptotic giant branch stars.

The largest known planetary nebula, the Helix Nebula, is $15'$ in diameter. However, the majority of those known are under $1'$ in size. All of the objects presented in this work are of a larger size and are not planetary nebulae.

A search for planetary nebulae using an Hα survey is being undertaken by Parker et al. (1999) in the Galactic plane. So far they have discovered over 700 candidates from 50% of the survey. Confirmatory spectroscopy has already been obtained for over 300 of these.

2.1.2 Supernova Remnants

Supernovae result from the core collapse of stars more massive than $\sim$3 $M_\odot$ (types Ib,II), or the explosion of a white dwarf due to accretion leading to the star exceeding the Chandrasekhar limit (type Ia). Material in the surrounding ISM is heated by the expanding shock wave producing filamentary shell structures in optical emission. They may be visible for a few times 10^5 years. The largest of these are over 100 pc in size. A summary of the physical parameters of several

well studied optical SNR in our galaxy is given in Lozinskaya (1992).

The optical morphology and spectra of known SNRs shows a great variety of types which depend on:

- the type of supernova outburst
- the influence of any stellar remnant
- the nature of the surrounding ISM
- a contribution from circumstellar material from the progenitor star
- the evolutionary stage of the remnant

Mathewson et al. (1983) have shown from a study of SNRs in the Magellanic Clouds that they can be separated into 4 classes: Balmer-dominated, oxygen-rich, plerionic-composite and evolved, that we detail below. Weiler & Sramek (1988) propose a fifth class, centrally-influenced. Details on individual objects may be found in Lozinskaya (1992) and Green (2000).

The Balmer-dominated remnants of Tycho, Kepler and SN 1006 are believed to result from type Ia supernovae, however the Ib class cannot be ruled out. Their spectra are strong in the hydrogen Balmer lines, but weaker in [S II], [N II] and [O III] than the typical evolved case . This results from a non-radiative shock meeting partially neutral gas (Chevalier & Raymond 1978).

Oxygen-rich remnants are distinguished by the presence of filaments with strong [O III] lines and in many cases lines of neon, argon and sulphur. The most studied example is Cassiopeia A; the spectra of its fast moving knots vary widely from feature to feature (Chevalier & Kirshner 1979). This material is ejecta from the explosion of a massive star, most probably within the last 2000 years (Lozinskaya 1992). Other examples are G292.0+1.8, Puppis A; N132D and 0540-69.3 in the LMC; 1E 0102.2-7219 in the SMC and an unresolved source in NGC 4449.

Plerionic and plerionic-composite remnants are classified as having filled-centre radio emission with a flat spectral index. Plerion-composite remnants have in addition an outer shell with a steeper spectral index (eg. Weiler 1983, Weiler & Sramek 1988). The main examples of the plerion class are the Crab Nebula and 3C 58 (SN 1181). Vela XYZ and W 28 are plerionic-composites. Many of these

have been shown to be strongly influenced by a pulsar, which may be true for the class as a whole. Optically these two classes display extended and filamentary emission throughout their centre.

The evolved remnants encompass the majority of known SNRs and may represent the final state of the other younger classes. They exhibit clear shell structure in optical and radio, and their optical spectra are dominated by Hα, [S II] and [N II] emission, produced by cooling behind the shock front. One of the best studied objects of this class is the Cygnus Loop.

Previous Optical SNR Searches

The most recent catalogue of Galactic SNRs (Green 2000) presents information on 225 SNR. Of these 156 are located in the southern sky. Optically, 20 of these SNRs have been detected in the southern sky compared with 31 in the northern sky. The smaller ratio in the southern sky is due to greater obscuration. By making deeper observations a greater proportion of these southern SNRs should be optically visible.

The first known SNRs were the brighter and closer objects such as the Crab and Vela remnants, of which several had obvious optical counterparts. Great advances in the sensitivity and resolution of radio surveys, especially in the late 1960s and more recently using interferometers, e.g. the Molongolo Observatory Synthesis Telescope (MOST) (Whiteoak & Green 1996), has resulted in most objects now being discovered by their radio emission.

Searches have been made to detect optical emission from radio SNR. The earliest comprehensive work was by van den Berg, Marscher & Terzian (1973) where the 24 then optically identified SNRs are detailed. Further identifications were made by van den Bergh from the late 1970s (van den Bergh 1976,1978,1979,1980). Another search from 1977 onwards, using UKST IIIaF and IIIaJ plates (Zealey, Elliott & Malin 1979), resulted in the first optical detection of many southern SNRs. Since then several other remnants have been optically identified, primarily through narrow band CCD imaging. References to these can be found in Green (2000).

2.1.3 Discrimination Between Formation Mechanisms

Optical Morphology as a Discriminator

Optical morphology can provide clues to the origin of filamentary structure, but it is only a guide. The presence of small knots and condensations, for instance, suggests ejected material associated with an oxygen-rich SNR, but this morphology may also be seen in Wolf-Rayet shells and planetary nebulae. The presence of filaments and diffuse emission throughout the centre may possibly indicate a plerionic object. Objects seen as partial or complete shell structures with a large angular size strongly suggest an evolved remnant. The effects of differing extinction levels and ISM structure from object to object makes classification from optical morphology alone impossible. In general optical spectroscopy, narrow-band imaging, and a radio spectral index are needed to reveal the true nature of filamentary objects.

Spectral Discrimination

In parallel with morphology, spectral information from radio and infrared observations can also be used to discriminate between the possible sources of the observed emission. The radio emission of SNR is produced by the synchrotron emission of relativistic electrons. This is non-thermal, and can be fit by a power law $S_\nu \propto \nu^\alpha$, with $-0.8 \leq \alpha \leq 0$ (Lozinskaya 1992). H II regions have a thermal spectrum, with $\alpha \sim 0$. Separation of the two processes can be made by direct measurement of the spectral index α. Linear polarization also indicates that the radio emission is synchrotron.

Better discrimination can often be made by comparing the 60 μm and radio emission from shells. Broadbent, Osborne & Haslam (1989) have shown a correlation between IRAS 60 μm emission from the Galaxy and radio continuum emission. From this it has been shown that the 60 μm to radio flux density ratio is high for H II regions and low for SNR, with both types being well separated. This method has been used with great success (e.g. Whiteoak & Green 1996) to identify SNR candidates.

2.2 The UKST Hα Survey

The Hα survey began in July 1997 on the UKST. Using 4° fields, 233 fields will cover the southern Galactic plane to a latitude of $|b| \leq 10°$, and 40 will be used for the Magellanic Clouds. Each exposure uses a 356 x 356 mm glass Hα interference filter with a central wavelength of 6590 Å and a FWHM bandpass of 70 Å. Although $6.5° \times 6.5°$ is imaged on each film, the filter is optimal within a circular diameter of 5.5°, and hence the usual 5° fields would not provide full coverage in the survey area. The three-hour exposures are taken on Tech Pan film, which offers improved sensitivity at the Hα wavelength and improved resolution in comparison with previous UKST R band surveys which used IIIaF emulsion. Further details of the survey and film are given Parker & Phillips (1998). The filter is described in Parker & Bland-Hawthorn (1998).

In February 1998 we began a systematic search of films produced by the Hα Survey. Films badly affected by trailing, poor focus, weather or other factors have not been closely examined as they will be repeated at a later date.

After an initial quick look to identify obvious large emission features, each film was visually scanned using a wide angle magnifying lens. This involved scanning horizontally across the film, working from the bottom of the field to the top, and ensuring that each strip overlapped so that no area was missed.

A wide variety of non-stellar objects are imaged on each film, primarily galaxies, planetary nebulae and diffuse H II regions. SNR and Wolf-Rayet shells optically have a filamentary appearance, and so can in general easily be distinguished from the above.

Digitized images of each object were then obtained, using a HP desktop scanner with transparency attachment. Approximate x-y positions of each object were measured off the film. These were entered into the UKST program PLADAT to obtain rough RA and Dec values. Using STScI Digitized Sky Survey images and the Karma program (Gooch 1996), each digitized image had a J2000 coordinate system attached to it. From this accurate positions were obtained for each object's centre and sizes were determined.

2.3 Discoveries

The most interesting class of objects identified are those over $30'$ in extent, with a filamentary appearance and a partially annular structure. At 5 kpc these objects would have diameters in excess of 40 pc. The larger of these are more likely to be identifiable as SNR, Wolf-Rayet or stellar wind shells, to be relatively close, and to be identifiable in other surveys.

From the fields examined so far, six such large objects have been identified. Two of these have been previously identified as SNR candidates from their optical emission, however they have been poorly studied and the Hα Survey has revealed far more extensive emission than previously recognized. A summary of these objects is presented in Table 2.1.

In addition we have identified many faint, isolated filaments under $10'$ in extent. Very few are identifiable with known objects. Unless identified as thermal through a large infrared flux or their radio spectral index, the best way of identifying these objects will be through deep imaging to reveal their full extent followed up with spectroscopy.

2.3.1 G245.9+0.9

This object is very faint on the original film. Computer enhancement shows a large amount of filamentary structure forming a full shell 1° in diameter (Figure 2.1). The emission is stronger towards the east. Radio continuum observations with the MOST at 843 MHz with resolution $43'' \times 43''$ cosec $|\delta|$ detected no significant radio emission from the object. However, it is visible, though faint and fragmentary, in 60μm images from IRAS (Beichman et al. 1985). From this there is a strong likelihood that the object is an H II region.

The Wolf-Rayet star HD 65865 lies interior to the shell at $7^{\rm h}59^{\rm m}46^{\rm s}$ $-28^\circ44'$ (J 2000), which is about $20'$ from the shell's geometrical centre. It has the spectral type WN5 and a distance of 4.61 kpc (van der Hucht 2000). This would imply a shell diameter of 107 pc if the shell is produced by this star, which lies within the range of shell diameters expected for Wolf-Rayet stars given by Marston (1997), from 1.3 pc to 180 pc.

2.3.2 G296.2-2.8

Here a nearly complete shell structure over 1° in diameter is visible (Figure 2.2). Some very fine and extended filaments exist along its western edge. A large amount of obscuration is evident interior to the shell. The bright nebula IC 2966 is also located within the shell at $11^{h}50^{m}15^{s}$, $-64°51'$ (J2000). Brand et al. (1986) list the nebula as BBW 374 in their catalogue. From CO measurements (Brand et al. 1987; Brand et al. 1993), the distance to IC 2966 is 3.28 kpc. Inside the nebula is the star VBH 56a (van den Bergh & Herbst 1975). It is of spectral type B0.5V, $V_0 = 11.47$, $V_0 - M_V$ ∼12.7, giving d ∼3.5 kpc. This indicates the star may be exciting IC 2966 but probably not the larger surrounding shell. If an association is real, using the distance to IC 2966 gives a size of ∼60 pc for G296.2-2.8.

A number of possible scenarios may explain the nature of this object:

1. The interaction of a SNR in the line of sight of the dark cloud and the cloud could produce a ring of filamentary emission.

2. The filamentary emission may represent a photodissociation region produced as the cloud is exposed to ionising radiation from a nearby source.

3. The filamentary shell may be the result of an SNR associated with the dark cloud.

4. The star VBH56a may be responsible for the bright nebula IC 2966 and the larger 1° shell, though the energetics make this unlikely.

A similar, but much closer object that may be compared with G296.2-2.8 is the Coalsack Loop (Walker & Zealey 1998), where a 10° ring of Hα emitting nebulosity surrounds the Coalsack Nebula. This loop is estimated to be between 33 pc and 43 pc in diameter. In this case weak radio emission has been identified with the shell, but there is again no obvious exciting source of the shell.

2.3.3 G304.7-3.1

G304.7-3.1 is an arc of filamentary emission (Figure 2.3) about 1° in size. The brightest of its filaments are towards the south-west, additional faint

filaments can be seen extending outside the figure to the north-east. These appear to be part of the northern edge of a larger diffuse emission feature which is clearly visible both optically and in the Parkes-MIT-NRAO (PMN) 4850 MHz survey (Griffith & Wright 1993). This diffuse optical emission directly overlays the radio emission which forms the 9° radio/Hα shell G303.5+0 surrounding the Coalsack (Duncan et al. 1995, Walker & Zealey 1998). The sharp filaments lie just inside this shell and may be part of the same shell.

These filaments have been associated with the WC6 type Wolf-Rayet star θ Mus (HD 113904) (Heckathorn et al. 1982) which lies about 30′ to the north. Its distance has been measured as 2.27 kpc (van der Hucht 2000). Imaging and spectroscopy (Giménez de Castro & Niemela 1998) show the filaments to be bright in Hα and [O III] while weak in [S II], and to have line ratios consistent with H II regions.

As the visible structure forms only a small part of a possible shell, an association with θ Mus must remain uncertain.

2.3.4 G310.2-2.8

The extensive isolated emission of this object is the most unusual in our sample. A main body of faint filamentary emission is seen to extend for ∼1.5°, along with two small patches of emission separated from this by ∼20′ (Figure 2.4). This object is visible in the PMN radio survey, one of the small Hα filaments corresponding with bright extended radio emission at $13^{\rm h}55.5^{\rm m}$ $-64°35'$ (J2000). The filament appears projected on the large 2.7° × 3.5° radio shell G310.5-3.5 (Duncan et al. 1997), and so we may be seeing optical emission from the front or back edge of the shell. In addition images taken with Mike Bessell's wide field imaging equipment at Siding Spring Observatory (Buxton et al. 1998) clearly show the optical emission in Hα and [S II] (6716Å,6731Å), indicating the presence of shock excited material. This region has been imaged with the Australia Telescope Compact Array (ATCA) (Roy Duncan 1998, private communication), showing the presence of polarized and non-thermal emission.

A radio image of the region, centred on $13^{\rm h}57^{\rm m}31^{\rm s}$, $-63°54'$ (J2000) has also been obtained on 3 April 1997, using MOST (Figure 2.5) at a frequency of 843 MHz in its wide-field mode. In this mode the field size is $163' \times 163'$ cosec $|\delta|$,

the rms noise level is 1-2 mJy beam^{-1} and the resolution (FWHM) is $43'' \times 43''$ cosec $|\delta|$. Further details of the MOST telescope and its operating modes are given in Bock et al. (1999) and references therein. Diffuse emission is visible over about $10'$ diameter at the same location as seen in the PMN radio survey, peaking at $\sim$5–7 mJy beam^{-1}. A faint arc of emission is visible just north of this at declination $-64°20'$. This image structure is very similar to that seen with the ATCA. The lines across the middle and along the bottom are grating ring artifacts from bright radio sources.

The general impression is that the diffuse optical emission matches radio features at $13^{\rm h}55.5^{\rm m}$ $-64°35'$ and possibly at $14^{\rm h}00^{\rm m}$ $-65°$. However the crisp filamentary structure visible optically has no counterpart in the radio. Further work on this object will be needed with improved sensitivity and resolution in order to detect the full extent and to establish a link between the optical and radio emission. While it is clear we that we are seeing an SNR in radio emission, a physical link with the optical emission needs to be established.

2.3.5 G340.5+0.7

Zealey et al. (1979) noted the presence of optical filaments west and northwest of the teardrop shaped globule Barnard 235 near the SNR G340.4+0.4. An image of this region obtained for the Hα survey shows very clearly this brighter filament, whose shape closely matches the shape of the edge of the globule, and fainter filaments to the north west of this filament (Figures 2.6 and 2.7). Additional filaments are located to the north of the bright filament in a region of enhanced emission (Figure 2.8). Some very faint features below this emission region can only be seen on the film.

The arc of emission close to the globule could be due to photoionisation by a nearby source or a supernova shock. The associated filamentary emission to the north, well away from the globule, makes a supernova shock more likely. It is possible that we are seeing extended emission from the western edge of a shell structure $\sim 20'$ in size. Unfortunately no related emission is visible in available radio surveys or IRAS data.

2.3.6 Kes 45

Kes 45 (G342.1+0.1, MSH 16-48, MHR 58) is a 30′ diameter radio source located at $16^{\rm h}53^{\rm m}46^{\rm s}$ $-43°35'$ (J2000). It has been considered an SNR based on its spectral index $\alpha = -0.50$ at 1 GHz (Milne 1970), although subsequently it has been lost from SNR catalogues.

Improved resolution radio observations (Caswell & Clark 1975) resolved several sources in this region. Two of these, G341.9-0.3 and G342.0-0.2, are now known to be SNR. However, as noted, the low frequency flux density of these sources is much less than the MSH flux density (Mills, Slee & Hill 1960), so an extended object is likely to be present.

Optically, images of the region show a network of filaments over an area 30′ in diameter (van den Bergh et al. 1973; Zealey et al. 1979) interacting with elephant trunk structures (Frieman 1954), instabilities that can form in expanding shock and ionisation fronts. Spectra in the visible region (Danziger & Dennefeld 1974; Danziger & Dennefeld 1976) indicate enhanced [S II] emission relative to Hα and weak [O III] 5007 Å emission, but the underlying H II region makes any interpretation very difficult.

Hα survey images show filamentary emission covering an area 1.5° in diameter. The main features are indicated in Figure 2.9. In Figure 2.10 a closeup is shown of the western group of filaments identified by van den Bergh et al. (1973). These filaments indicate an association with a dark cloud in the shell of NGC 6231. New features include two filaments to the east located near $17^{\rm h}00^{\rm m}$, $-44°00'$ (J2000), and a large number of filaments to the northeast, a section of which is shown in Figure 2.11.

If these optical filaments represent a single object, then the diameter, assuming an association with the NGC 6231 H II region to the north (Zealey et al. 1979), becomes 36 pc.

The combination of size, extensive optical emission and low radio flux indicate that Kes 45 is in an advanced state of evolution.

2.4 Conclusions

Using films from the AAO/UKST Hα Survey we have identified four large filamentary shell structures, one of these a new possible Wolf-Rayet shell, and new optical emission in two known SNR candidates. These objects are:

- G245.9+0.9, a faint $1°20'$ optical shell surrounding the Wolf-Rayet star HD 65865
- G296.2-2.8, a $1°$ optical shell with interior absorption, possibly associated with the star VBH 56a
- G304.7-3.1, an arc of filamentary emission on the edge of a larger shell structure, and likely associated with θ Mus
- G310.2-2.8, a filamentary structure with an unusual morphology and associated radio emission
- G340.5+0.7, a small patch of optical filaments
- Kes 45, a system of optical filaments $1.5°$ in diameter, which has long been suspected as an SNR

Techpan film used with the new Hα filter is detecting fainter and more distant filamentary structures in comparison with previous photographic surveys, due to the improved spatial resolution, red sensitivity of the film, and narrow bandpass of the filter.

Based on the discovery rate and survey completion, we expect that 16 or more large filamentary structures may be discovered by this survey.

2.5 Acknowledgements

We would like to thank the UKST staff for obtaining and making available the films used in this work, and providing the opportunity for A. Walker to observe at the UKST during the first half of 1998. We would also like to thank the referees whose helpful comments greatly improved this paper. The Digitised Sky Surveys were produced at the Space Telescope Science Institute under US

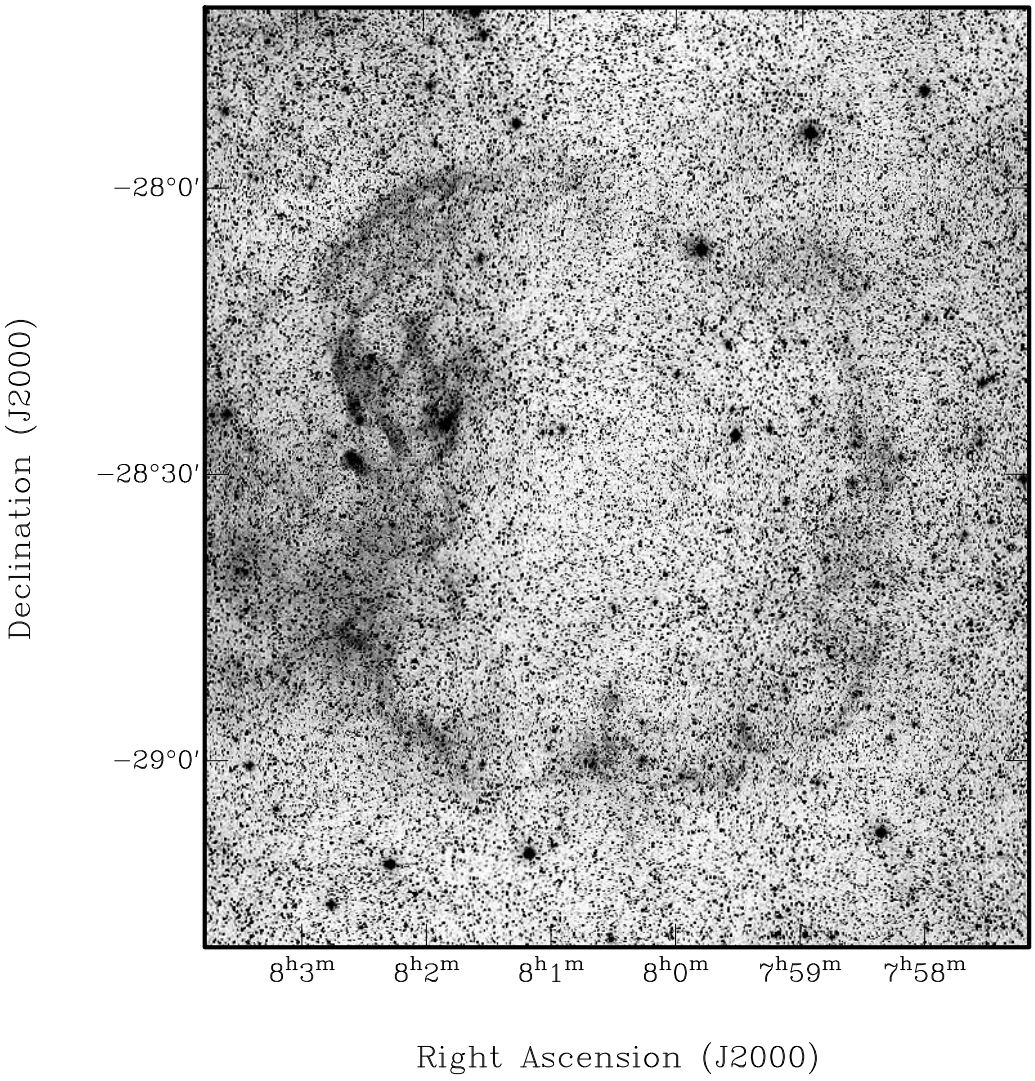

Figure 2.1: G245.9+0.9

Government grant NAG W-2166 based on photographic data obtained using the Orsin Schmidt Telescope on Palomar Mountain and the UK Schmidt Telescope. The UK Schmidt Telescope was operated by the Royal Observatory Edinburgh, with funding from the UK Science and Engineering Research Council until 1988 June, and thereafter by the Anglo-Australian Observatory. The MOST is operated by the University of Sydney with support from the Australian Research Council and the Science Foundation for Physics within the University of Sydney.

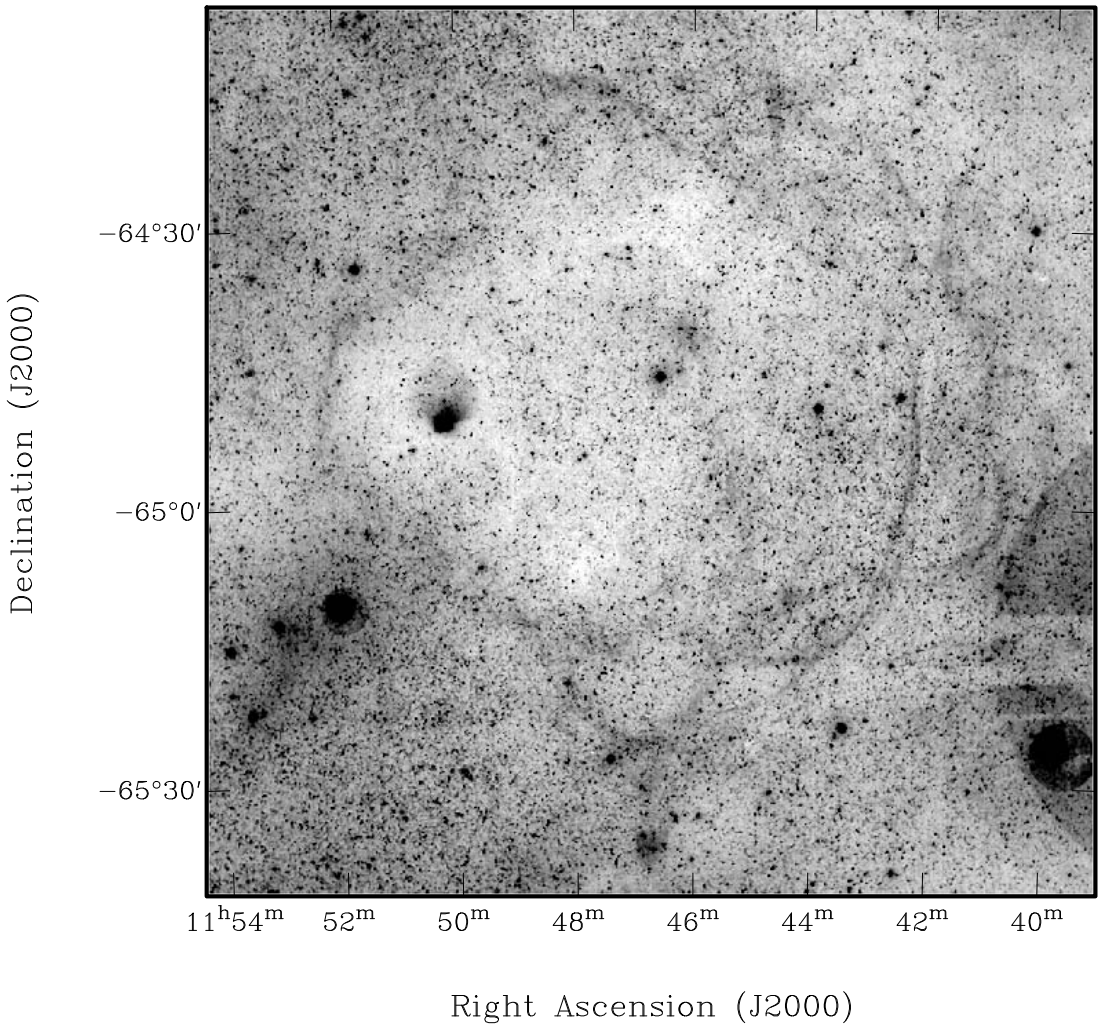

Figure 2.2: G296.2-2.8

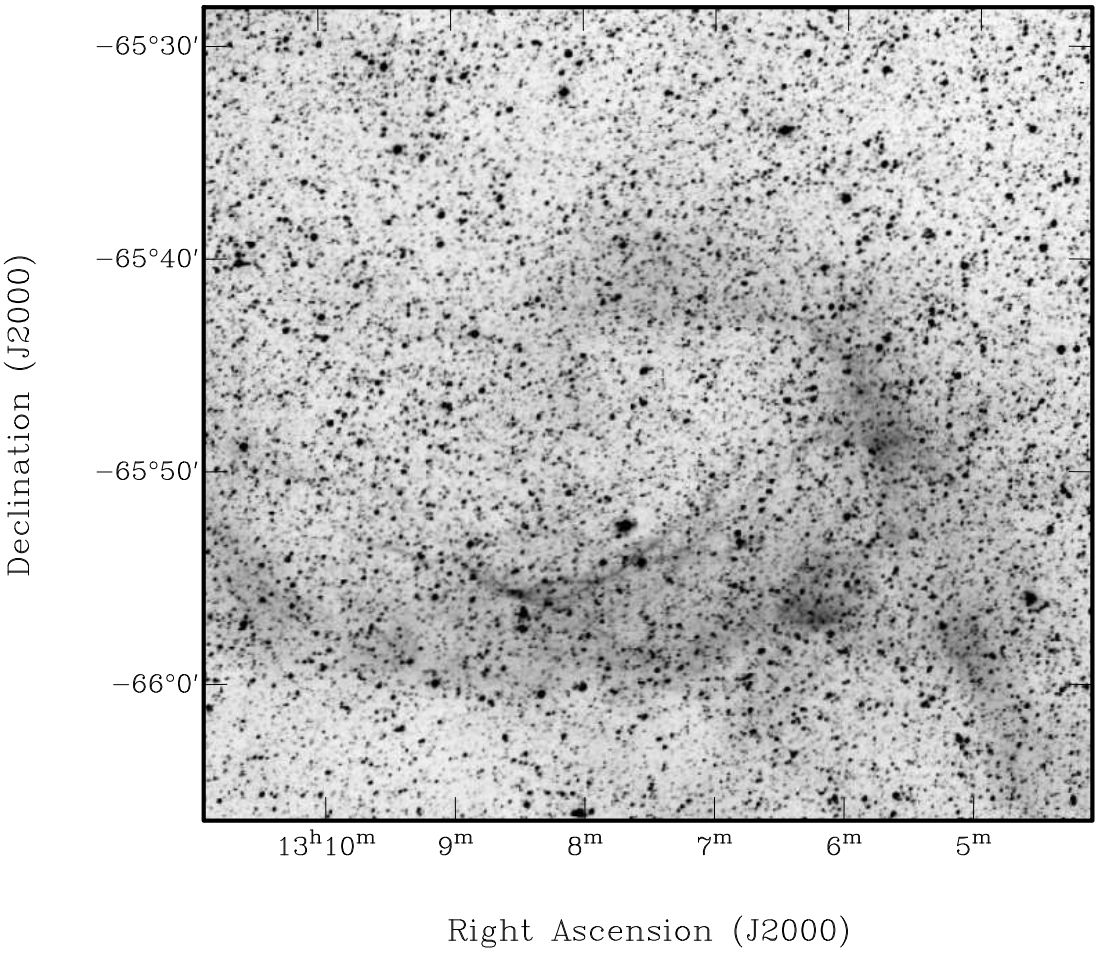

Figure 2.3: G304.7-3.1

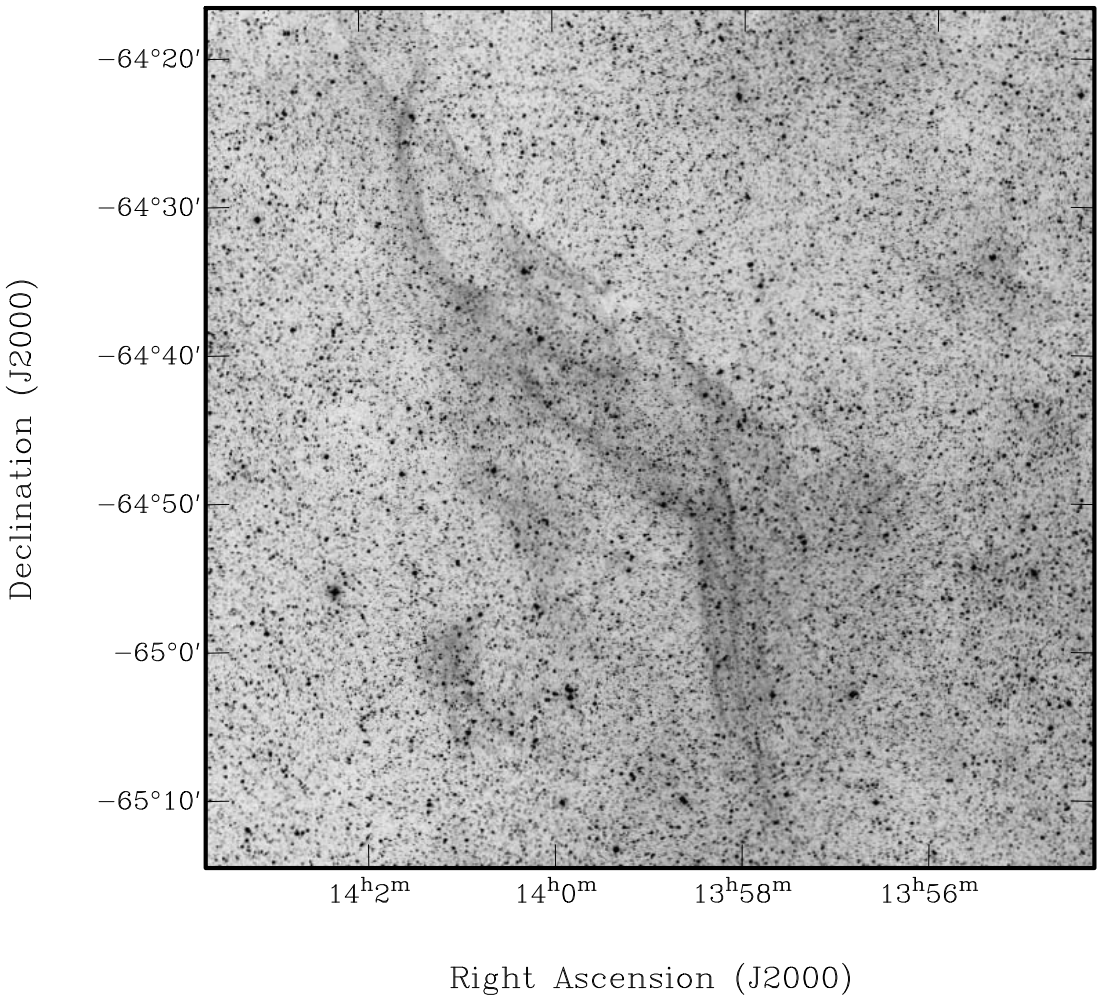

Figure 2.4: G310.2-2.8

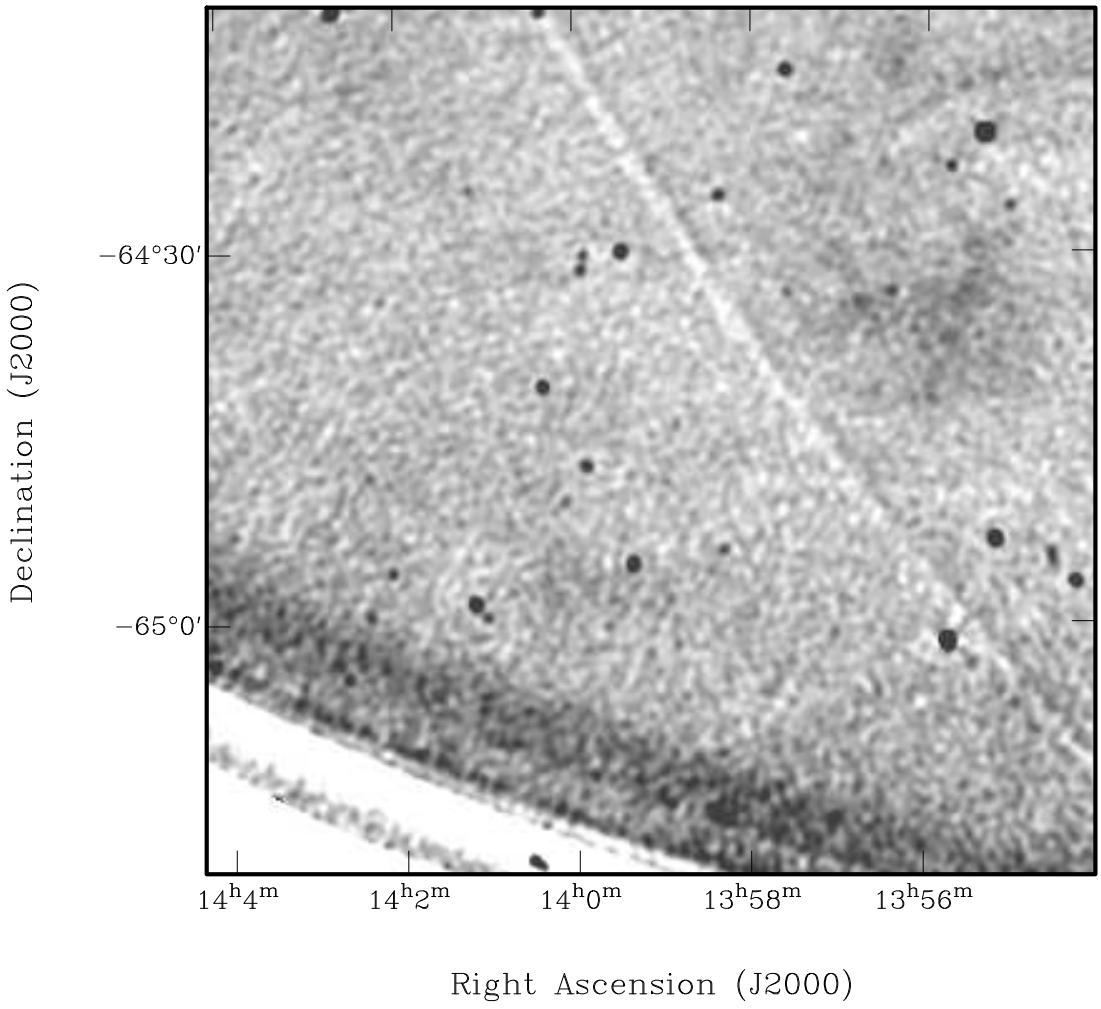

Figure 2.5: MOST image of G310.2-2.8

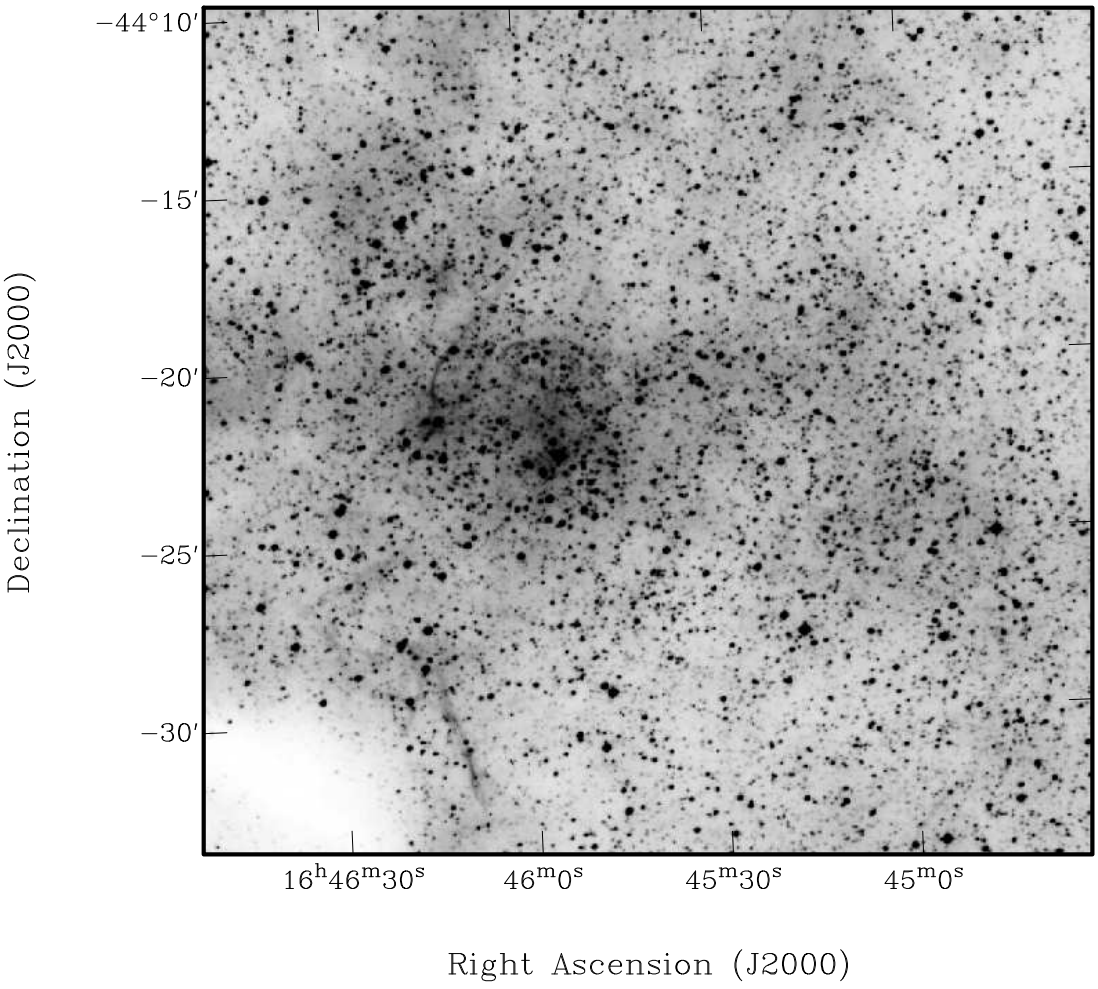

Figure 2.6: G340.5+0.7

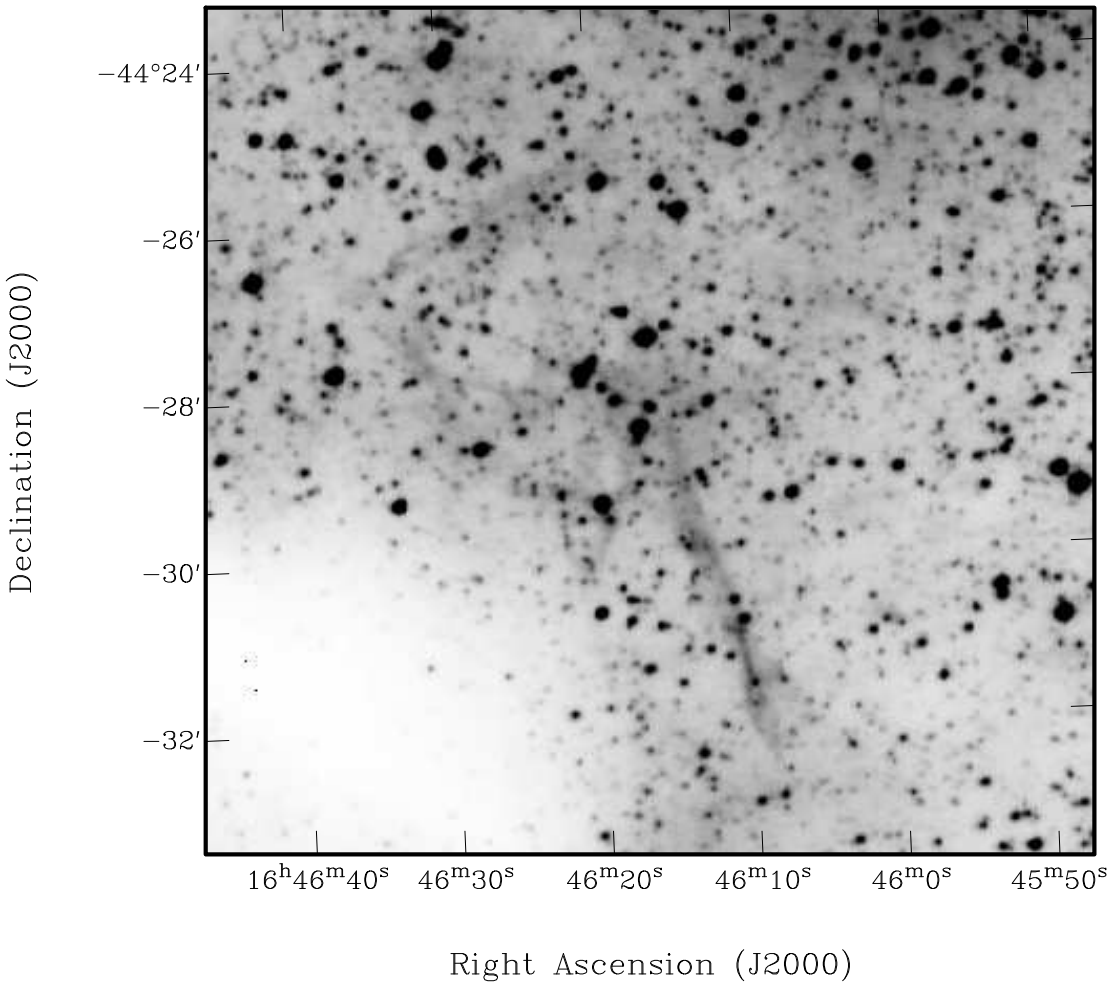

Figure 2.7: Closeup of southeast quadrant of G340.5+0.7

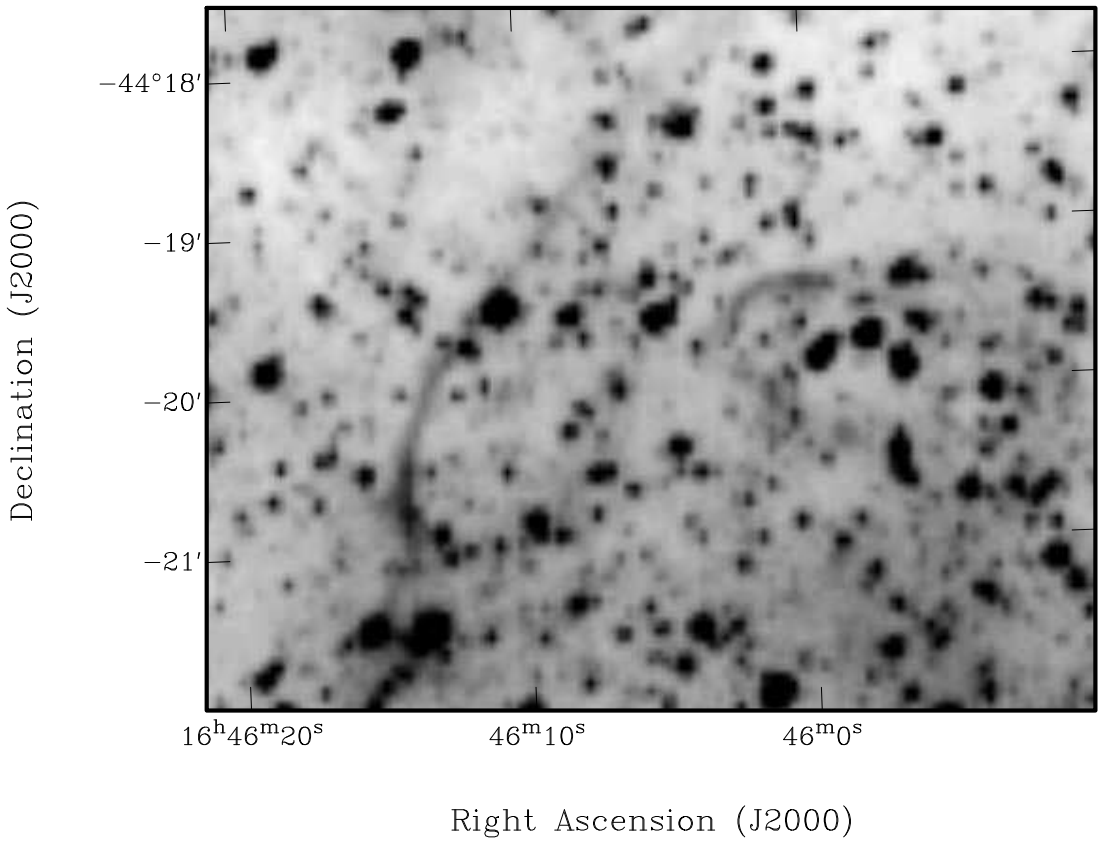

Figure 2.8: Closeup of northeast quadrant of G340.5+0.7

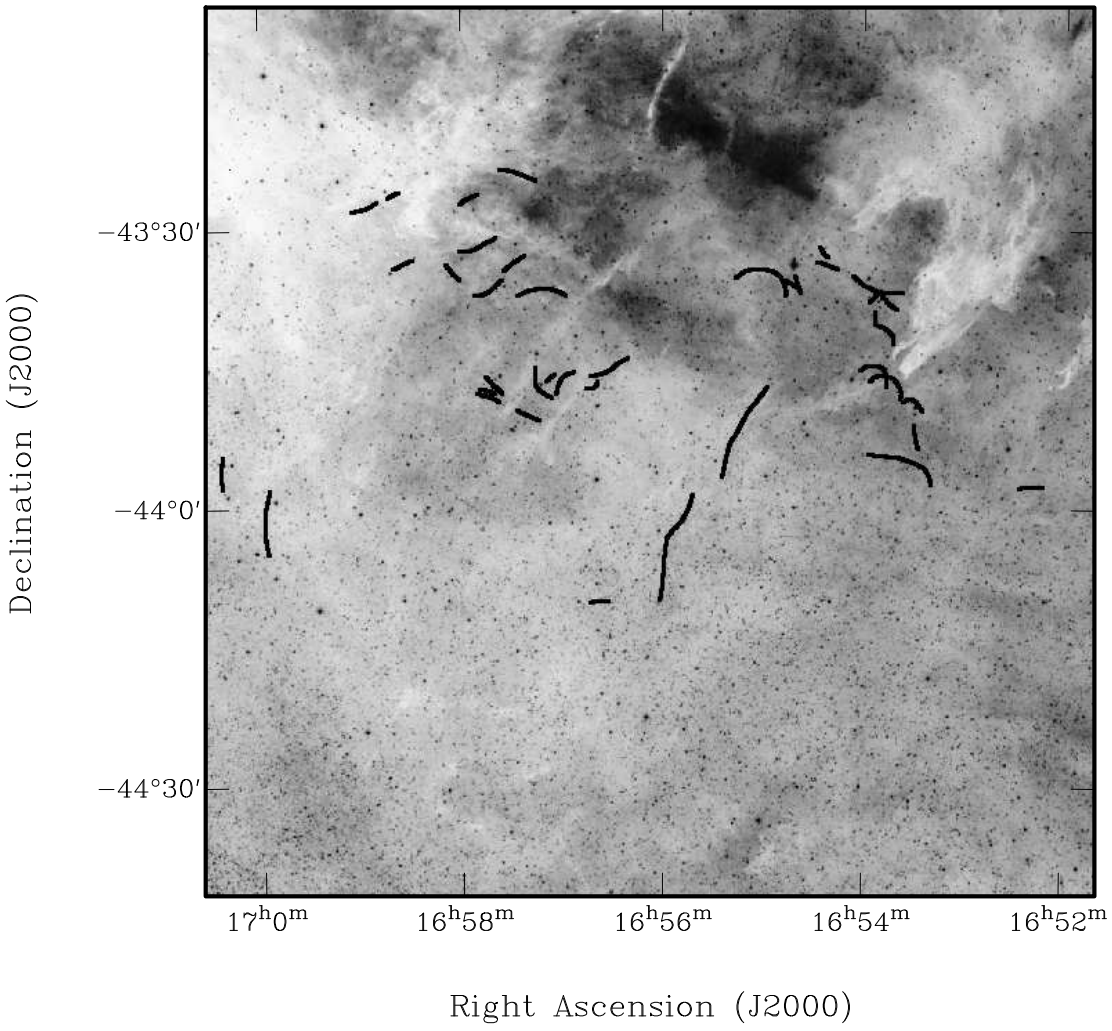

Figure 2.9: Diagram showing major filamentary structures in the Kes 45 region.

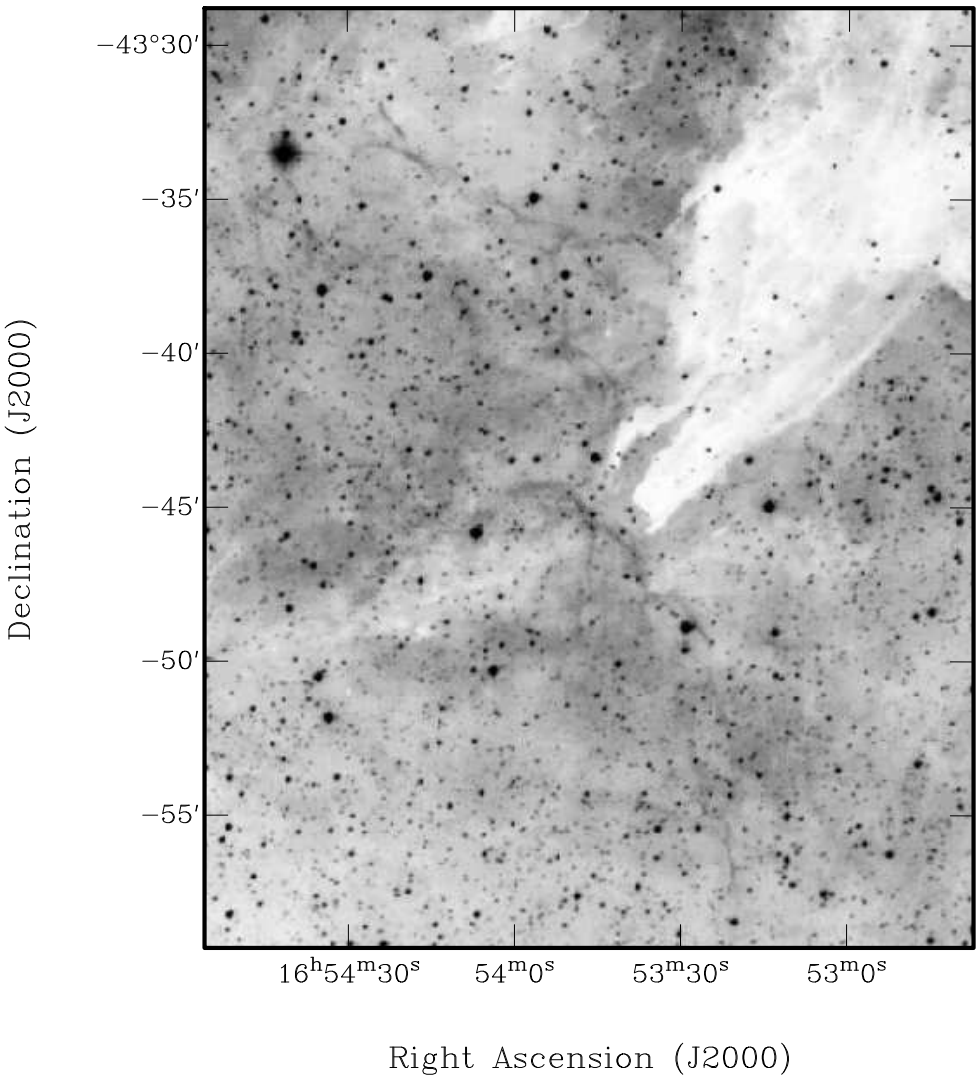

Figure 2.10: Closeup of central western section of Kes 45.

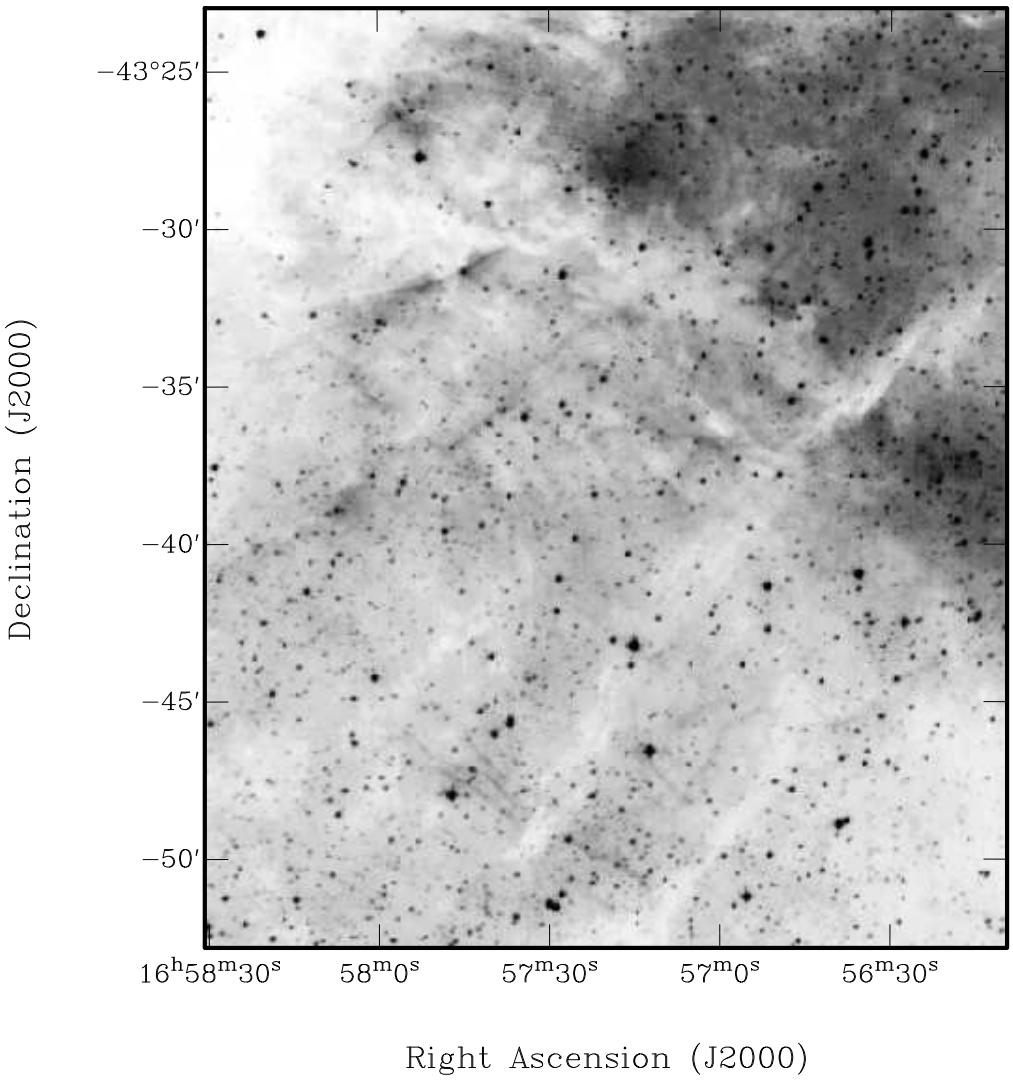

Figure 2.11: Closeup of northeast quadrant of Kes 45.

Table 2.1: Filamentary structures

Object	R.A. (2000.0)	Dec. (2000.0)	Approximate size	Comments
G245.9+0.9	$08^{h}00.5^{m}$	$-28°30'$	$1°20'$	New WR shell
G296.2-2.8	$11^{h}47^{m}$	$-64°50'$	$1°$	
G304.7-3.1	$13^{h}08^{m}$	$-65°56'$	$1°$	θ Mus
G310.2-2.8	$14^{h}00^{m}$	$-64°45'$	$1° \times 1°30'$	
G340.5+0.7	$16^{h}46^{m}$	$-44°25'$	$20'$	Possible SNR
Kes 45	$16^{h}56^{m}$	$-43°45'$	$1°30'$	Possible SNR

Positions given are geometric centres of the observed emission.

Chapter 3

Multifibre Spectroscopy of the Supernova Remnant Candidate RCW 114

This chapter is based on published material Walker et al., 2001, "Multifibre Spectroscopy of the Supernova Remnant Candidate RCW 114", MNRAS, **325**, 287.

3.1 Introduction

RCW 114 is a filamentary nebula of about 250 arcmin diameter located at RA (1950) = $17^{\rm h}$ $23^{\rm m}$, Dec. (1950) = $-46°$. An Hα exposure taken with the UK Schmidt Telescope shows the presence of filamentary emission around its full circumference, with less emission visible in the centre (Meaburn & Rovithis 1977). The presence of filaments down to 10 arcsec in width, along with an increase in the 29.9 MHz radio brightness in this region, led to their suggestion of this object being a supernova remnant (SNR).

Later work provided further evidence for this identification. Bedford et al. (1984) measured the interstellar Na I line at 5890Å using the light of seven B stars coincident with and outside the nebula. These give RCW 114 a distance of $<$200 pc, a diameter of $<$17.5 pc, and an age of $\sim 2\times10^4$ yr.

Meaburn et al. (1991) obtained Hα profiles in four positions. These show the nebula to be expanding at $V_{exp} = 25 - 35$ km s^{-1}. In addition, their

calculation of the kinetic energy of the shell, based on far-infrared flux densities from IRAS scans, gives a value consistent with that produced by a Type II supernova.

Presently RCW 114 is catalogued as a possible supernova remnant (Green 2000) with the identification G343.0-6.0. As discussed by Bedford et al. (1984), positive identification as a supernova remnant has not been possible, as a result of the non-detection of soft X-ray emission and the apparent absence of non-thermal radio emission. It has also been suggested that RCW 114 is associated with the Wolf-Rayet star HD 156385 (WR 90) (Cappa de Nicolau et al. 1988), however the star is far beyond RCW 114 at $\sim$2 kpc (Bedford et al. 1984).

We have examined a 4850 MHz radio map of this area from the Parkes-MIT-NRAO survey (Griffith & Wright 1993). This clearly shows weak emission which strongly corresponds with the optical structure seen in Hα emission. In addition, RCW 114 has also been identified at 2.4 GHz (Duncan et al. 1997), with the suggestion being made that it is a non-thermal source.

In light of this evidence, it seemed highly appropriate and timely that further study be made of this object. Here we present a spectroscopic study of RCW 114 conducted with the FLAIR instrument on the UK Schmidt Telescope. Our work is based on emission-line strengths and unambiguously shows that RCW 114 is a supernova remnant.

3.2 Observations and Reductions

A 120-min exposure of RCW 114 centred on RA (1950) = $17^{\rm h}$ $20^{\rm m}$, Dec. (1950) = -46° was obtained in 1997 August with the UK Schmidt Telescope. This used the new Hα filter (Parker & Bland-Hawthorn 1998) and Tech Pan film in order to record faint and fine details within the nebula.

The FLAIR fibre-optic system (Parker & Watson 1995) allows the observer to obtain spectra from up to 92 objects simultaneously within the telescope's field of $6^\circ \times 6^\circ$. This is ideal for this study because of the large angular size of the object, and because a large representative sample of the filaments of the object can be observed. In practice, when obtaining line ratios or fluxes for emission-line objects, less than half this number can be observed, as a result of a small light leakage between adjacent fibres. A film copy of the RCW 114 Hα

image was made. This was used to select filaments to be observed. The film was attached to a metal backing-plate and the prism on the end of each fibre attached to the film in the position to be observed. This is then loaded into a plateholder for use in the telescope as described in Parker & Watson (1995).

Spectra were obtained at 34 object positions, other fibres were used for sky subtraction and image guiding on fiducial stars. The sky subtraction positions were chosen around the field in small regions free from stars with as little background emission as possible outside the main filamentary structure. Details of observations made are given in Table 3.1. For all observations the gratings were used "blaze-to-camera". In addition bias frames, arc frames and dome flats were obtained.

The data was reduced using the IRAF package, following a standard procedure developed for FLAIR data. The first main step is bias and flat correction using the CCDPROC procedure. The corrected frames for each observation are then combined. The DOFIBERS procedure is used to define apertures for each fibre spectra, which are traced along the dispersion axis. Dome flats are then used to correct for the efficiency of each fibre. Wavelength calibration is made using the arc frames. Corrected spectra are then extracted and sky-subtracted, using an average of the sky spectra. A correction for the wavelength response of the system was also made by comparing domeflats with black body curves calculated at the lamp temperature.

3.3 Results

Representative spectra are shown in Figures 3.1 and 3.2. In the red, the spectra are dominated by the Hα λ6563, [N II] $\lambda\lambda$6548, 6583 and [S II] $\lambda\lambda$6717, 6731 lines. The close pairs are only partly resolved with the 300B grating, but are clearly separated with the 600V grating. Emission from the [O I] and Na I lines is also visible: however, sky subtraction on these is generally poor, as seen on comparison of the high- and low-resolution spectra.

The blue end of the spectra is dominated by the Hβ, Hγ and Hδ lines. In addition some spectra show evidence of weak emission from [O III] $\lambda\lambda$4949, 5007 and [Fe II], however these are for the most part not far above the noise level. Below 4250-Å wavelengths, many of the spectra are very noisy and show a sloped

continuum, as a result of the low system response in this region. In addition the $100 - \mu$m width of the fibres led to stellar contamination in some spectra.

SPECFIT in IRAF was used to construct a model of the data in the wavelength range 6500–6750 Å. This consisted of a linear continuum background and Gaussian line profiles. Once a fit has been obtained to a desired accuracy level, it is possible to produce a list of fit parameters and errors calculated using the error spectra.

To estimate the error spectra, the following procedure was used. The square root was taken of each pixel of the combined data frame (before the IRAF DOFIBERS task was used). This was then divided by the square root of the number of frames, to estimate the error at each pixel. The result was processed with the DOFIBERS procedure in the same manner as the data frames, except that no sky subtraction was performed. From these error spectra, a table was produced for each separate set of spectra, listing the wavelength, flux value and estimated error of the flux at each data point

To obtain more accurate line ratios, it was intended to correct line fluxes for interstellar reddening. This involves assuming an intrinsic Hα/Hβ ratio of 3.0, and applying a correction based on the observed ratio. The observed ratio should be greater than 3.0, however in our response-corrected spectra the ratio was often much lower. This is likely to be a result of the lamp temperature being in error or the lamp deviating from a black body curve. As a result, no reddening corrections have been made. Our [S II]/Hα results are still reliable, because of the small wavelength range involved and the proximity of RCW 114. Provided the reddening is not extreme, an examination of published results for this line ratio in SNR shows that ignoring reddening produces an error of only a few percent in more reddened objects.

As a result of the position at which the sky spectra were taken, the subtracted spectra represent a combination of emission filaments and a more diffuse component from any extended nebulosity. The latter is below a few percent of the intensity of the filamentary emission, and has only a small effect on the [S II]/Hα ratios.

3.4 Line Diagnostics

The most widely used supernova remnant diagnostic involving emission-line strengths is the [S II]$\lambda\lambda$6717, 6731/Hα line ratio (Fesen, Blair & Kirshner 1985). When this ratio is observed to be greater than 0.5, it indicates the emission is being produced by shock-excited gas which has been swept up by a low-velocity shock. This can be compared with H II regions and planetary nebulae, where this ratio is usually much smaller, and Hα is predominant. Unfortunately, the highest values of the ratio in these objects overlap the lowest values observed in SNR. In addition, [S II] emission may be very weak or absent in Balmer-dominated filaments [produced by high-velocity shocks travelling through an intercloud region, e.g. RCW 86 (Long & Blair 1990, Smith 1997), and the Cygnus Loop], and in oxygen-rich SNR (Weiler & Sramek 1988). Fesen et al. (1985) examine a number of other useful emission-line ratios, mainly involving oxygen and hydrogen lines.

In Table 3.2 we show the calculated line strengths for the five major lines in the red spectrum, along with some derived ratios. The line strengths have been scaled to Hα = 100. The errors were determined as discussed above. The filaments observed were seen to cover a wide range of values for the [S II]/Hα ratio, from a minimum of 0.20 to a maximum of 1.17. About half of these ratios are in the range 0.5-0.7. While some of the weaker features will have large errors, a large ratio was also observed in some of the stronger-emitting filaments. This indicates that the emission seen in RCW 114 is predominately produced by shock excitation.

3.5 Optical Images

In order to further examine the ionization structure of RCW 114, narrow-band images were taken with Mike Bessell's wide field imaging equipment (Buxton, Bessell & Watson 1998) at Siding Spring Observatory during 1998. The images were obtained using a 400-mm f/4.5 Nikkor-Q lens and a 2K $\times$ 2K SITe thinned CCD. Each pixel is 12 arcsec in size, the full image covers 7°$\times$7° of sky. Four 10-min exposures were taken of RCW 114 with each of the filters Hα 55Å (6563Å), [S II] 25Å (6732Å), [O III] 25Å (5016Å) and red continuum 55Å (6676Å). Each image was processed using standard IRAF tasks. After bias, flat-field and

dark-frame corrections, images were aligned and then combined.

No structure was visible in the [O III] or red continuum images. The Hα and [S II] images were continuum-subtracted and had a 3x3 median filter applied to remove most of the remaining stellar images. While the [S II] emission is weaker, there is very little difference in the visible structure in both bands.

3.6 Spatial Variation

In Figures 3.3 and 3.4 we have plotted the [S II]/Hα and [N II]/Hα ratios respectively at each of the fibre positions, using the Hα image described in Section 3.5. The first of these appears to be larger along the bright eastern filament, and smaller for the south-western filaments. The three measured filaments to the north-west have ratios typical of H II regions, while the single northern ratio is strong. These values show that the expanding shock is interacting more strongly with the ISM away from the Galactic plane, which lies to the north-west. No such clear pattern is visible in Figure 3.4.

Two positions in the south-east stand out for having unusually high values for both of these values. The first is at RA (1950) = $17^{\rm h}\ 32^{\rm m}\ 51^{\rm s}$, Dec. (1950) = $-46^\circ\ 48'$ on a long, faint filament, and the second at RA (1950) = $17^{\rm h}\ 27^{\rm m}\ 10^{\rm s}$, Dec. (1950) = $-47^\circ\ 26'$ on a very small but bright filament. It is likely that these are in some way related and lie in front of or behind the other emission in this area.

3.7 Discussion

By comparison with spectra of known remnants (Fesen et al. 1985), it can be seen that our results are consistent with spectra of an evolved SNR. This is also suggested by the weak radio emission which appears to trace the optical structure. This can be contrasted to the younger Vela SNR, where the radio flux is stronger, [O III] emission is strong, and their is less correlation between optical and radio emission (Cram, Green & Bock 1998).

In Table 3.3 we present a list of all known large angular diameter (100 arcmin or more) SNR within the galaxy, including RCW 114. Of these RCW 114 is both the nearest and of the smallest physical size. As expected, the remnants

with optical emission are generally closer. In contrast, despite being the closest, RCW 114 has weak radio emission. This, and its small physical size despite being well evolved, are suggestive of a weak initial explosion. This was also suggested by Bedford et al. (1984); however, their figure for the initial energy of 2×10^{47} erg was later shown to be erroneous (Meaburn et al. 1991). Another possibility is that the remnant is expanding into a dense medium, and that after $\sim2\times10^{4}$ years the shock has diminished sufficiently so that radio emission is weaker and radiative cooling still significant.

The large angular size and extensive optical emission of RCW 114 will allow it to be studied in detail and greatly improve our knowledge of evolved SNR. In the future it will be important to obtain single-slit observations of some filaments, in order to confirm these results. Better sky subtraction will be possible, allowing us to obtain results on the oxygen lines and detect other fainter lines. These will be essential for a proper comparison with other evolved SNR.

We have also applied to obtain radio maps of small sections of RCW 114 using the Molongolo Observatory Synthesis Telescope (MOST), which has proved to be excellent in detecting extended non-thermal emission from SNR (Whiteoak & Green 1996). This will allow us to examine the relationship between Hα and radio emission in both position and strength. It will also provide a second test of the SNR identification by comparison with IRAS data. In the longer term, an investigation of the radio continuum emission from RCW 114 will be useful. Links that can be established between observed properties in different wavelength regions will give a new insight into the processes and conditions within SNR.

3.8 Conclusions

We have shown that the optical emission being produced by RCW 114 is consistent with that expected of an evolved supernova remnant as suggested by earlier studies. This is confirmed by the weak radio emission and lack of detectable [O III] emission. A wide range of [S II]/Hα ratios have been observed, suggesting that the interstellar medium into which it is expanding is non-uniform. This study has shown that the FLAIR fibre-optic system is very useful for the study of large and extended emission-line objects.

Table 3.1: Details of FLAIR Observations

Grating	Central wavelength (Å)	Wavelength range (Å)	Instrumental resolution (Å)	CCD Resolution (Å/pixel)	Date	Frames
600V	6052	5288–6815	4.4	2.9	1997 Aug 28	4 × 1800s
600V	4645	3926–5364	4.5	2.8	1997 Aug 29	3 × 1800s
300B	5554	4070–7038	9.3	5.6	1997 Aug 29	3 × 1800s

3.9 Acknowledgements

We would like to thank the staff of the UK Schmidt Telescope, especially Dr. Quentin Parker, for their help and advice in making these observations.

Table 3.2: Observed emission line strengths in RCW 114.

Position (B1950.0)				F(λ)			Line Ratios		
R.A.	Dec.	[N II]λ6548	H$\alpha\lambda$6563	[N II]λ6583	[S II]λ6717	[S II]λ6731	[S II]/Hα	[N II]/Hα	6716/6731
17 11 16	-46 13.9	17 ± 1	100 ± 1	55 ± 1	28 ± 1	18 ± 1	0.46 ± 0.01	0.72 ± 0.02	1.54 ± 0.08
17 11 19	-45 52.6	13 ± 1	100 ± 1	44 ± 1	19 ± 1	13 ± 1	0.32 ± 0.01	0.57 ± 0.02	1.38 ± 0.11
17 12 29	-45 14.3	15 ± 1	100 ± 1	44 ± 1	11 ± 1	9 ± 1	0.20 ± 0.01	0.58 ± 0.02	1.23 ± 0.16
17 13 34	-46 25.1	15 ± 1	100 ± 2	50 ± 1	24 ± 1	18 ± 1	0.41 ± 0.01	0.66 ± 0.02	1.37 ± 0.09
17 13 49	-44 56.4	14 ± 1	100 ± 1	47 ± 1	17 ± 1	12 ± 1	0.29 ± 0.01	0.61 ± 0.02	1.44 ± 0.12
17 14 31	-44 55.7	17 ± 1	100 ± 1	51 ± 1	22 ± 1	15 ± 1	0.36 ± 0.01	0.68 ± 0.02	1.50 ± 0.09
17 15 22	-46 06.9	18 ± 1	100 ± 1	53 ± 1	30 ± 1	19 ± 1	0.49 ± 0.01	0.71 ± 0.02	1.54 ± 0.07
17 15 25	-46 48.3	15 ± 1	100 ± 1	47 ± 1	19 ± 1	13 ± 1	0.31 ± 0.01	0.62 ± 0.01	1.47 ± 0.07
17 16 34	-46 04.3	15 ± 1	100 ± 2	51 ± 1	31 ± 1	21 ± 1	0.52 ± 0.02	0.67 ± 0.02	1.45 ± 0.09
17 16 42	-47 13.1	16 ± 1	100 ± 1	54 ± 1	26 ± 1	19 ± 1	0.44 ± 0.01	0.71 ± 0.02	1.36 ± 0.08
17 16 52	-45 31.9	17 ± 2	100 ± 3	59 ± 2	55 ± 2	39 ± 2	0.94 ± 0.04	0.75 ± 0.04	1.40 ± 0.08
17 18 57	-47 25.0	15 ± 1	100 ± 2	48 ± 2	30 ± 1	22 ± 1	0.51 ± 0.02	0.63 ± 0.03	1.38 ± 0.10
17 19 14	-46 38.6	14 ± 1	100 ± 2	50 ± 1	32 ± 1	22 ± 1	0.54 ± 0.02	0.64 ± 0.02	1.43 ± 0.07
17 19 40	-47 00.4	15 ± 1	100 ± 2	47 ± 1	27 ± 1	19 ± 1	0.46 ± 0.02	0.62 ± 0.02	1.46 ± 0.09
17 20 17	-47 46.8	15 ± 1	100 ± 2	57 ± 2	38 ± 2	24 ± 2	0.63 ± 0.03	0.72 ± 0.03	1.57 ± 0.12
17 22 18	-45 39.2	21 ± 2	100 ± 3	59 ± 2	37 ± 2	22 ± 2	0.58 ± 0.03	0.80 ± 0.04	1.68 ± 0.16
17 22 23	-46 17.8	19 ± 1	100 ± 2	58 ± 2	30 ± 1	20 ± 1	0.51 ± 0.02	0.77 ± 0.03	1.49 ± 0.12
17 22 46	-47 37.8	11 ± 2	100 ± 3	43 ± 2	30 ± 2	23 ± 2	0.53 ± 0.03	0.54 ± 0.04	1.30 ± 0.14
17 22 53	-43 40.1	14 ± 1	100 ± 1	48 ± 1	30 ± 1	22 ± 1	0.52 ± 0.02	0.62 ± 0.02	1.39 ± 0.07
17 23 03	-46 53.0	16 ± 1	100 ± 1	49 ± 1	33 ± 1	22 ± 1	0.54 ± 0.01	0.66 ± 0.02	1.53 ± 0.07
17 23 48	-48 12.3	10 ± 2	100 ± 3	43 ± 2	33 ± 2	21 ± 2	0.53 ± 0.03	0.54 ± 0.04	1.56 ± 0.17
17 25 29	-46 08.5	16 ± 1	100 ± 2	49 ± 1	35 ± 1	24 ± 1	0.59 ± 0.02	0.65 ± 0.02	1.43 ± 0.08
17 25 52	-46 39.2	14 ± 1	100 ± 1	43 ± 1	34 ± 1	24 ± 1	0.57 ± 0.01	0.57 ± 0.02	1.42 ± 0.06
17 27 10	-47 26.4	29 ± 1	100 ± 2	102 ± 2	67 ± 2	49 ± 2	1.16 ± 0.03	1.30 ± 0.04	1.38 ± 0.06
17 27 33	-47 47.0	12 ± 1	100 ± 2	42 ± 1	39 ± 1	29 ± 1	0.68 ± 0.02	0.53 ± 0.02	1.34 ± 0.07
17 29 13	-46 32.7	15 ± 1	100 ± 1	44 ± 1	30 ± 1	20 ± 1	0.50 ± 0.01	0.59 ± 0.01	1.47 ± 0.05
17 30 01	-46 11.2	15 ± 1	100 ± 1	42 ± 1	32 ± 1	23 ± 1	0.55 ± 0.01	0.57 ± 0.01	1.43 ± 0.05
17 31 39	-45 46.6	15 ± 1	100 ± 2	48 ± 1	41 ± 1	28 ± 1	0.69 ± 0.02	0.63 ± 0.02	1.50 ± 0.07
17 32 51	-46 48.2	19 ± 3	100 ± 4	59 ± 3	53 ± 3	42 ± 3	0.95 ± 0.05	0.78 ± 0.05	1.27 ± 0.11

Table 3.3: Large angular diameter supernova remnants.

Name	Diameter (arcmin)	Distance (kpc)	Distance Ref.	Diameter (pc)	Other names	Optical?
G 28.8+1.5	100	< 3.9	1	< 110		N
G 39.7-2.0	120×60	3.0	2	105×50	W 50	Y
G 65.3+5.7	310×240	$\sim$1.0	3	90×70		Y
G 74.0-8.5	230×160	0.8	4	54×37	Cygnus Loop	Y
G 89.0+4.7	120×90	0.8	4	28×21	HB 21	Y
G 152.2-1.2	110	6.6	4	210		N
G 156.2+5.7	110	3.0	4	96		N
G 160.9+2.6	140×120	2.2	4	90×77	HB 9	Y
G 180.0-1.7	180	1.5	4	79	S147	Y
G 205.5+0.5	220	1.6	4	100	Monoceros	Y
G 263.9-3.3	440	0.25	5	32	Vela	Y
G 330.0+15.0	180	1.2	4	63	Lupus Loop	Y
G 343.0-6.0	250	< 0.2	6	< 17.5	RCW 114	Y

All diameter values are from Green (2000) except for Vela which is from Aschenbach (1993). Bonsignori-Facondi & Tomasi (1979) quote a distance for G 152.2-1.2 of 1.6 kpc.

References: 1 - Schwentker (1994); 2 - Dubner et al. (1998); 3 - Fesen, Gull & Ketelsen (1983); 4 - Case & Bhattacharya (1998) and references therein; 5 - Chan, Sembach & Danks (1999); 6 - Bedford et al. (1984).

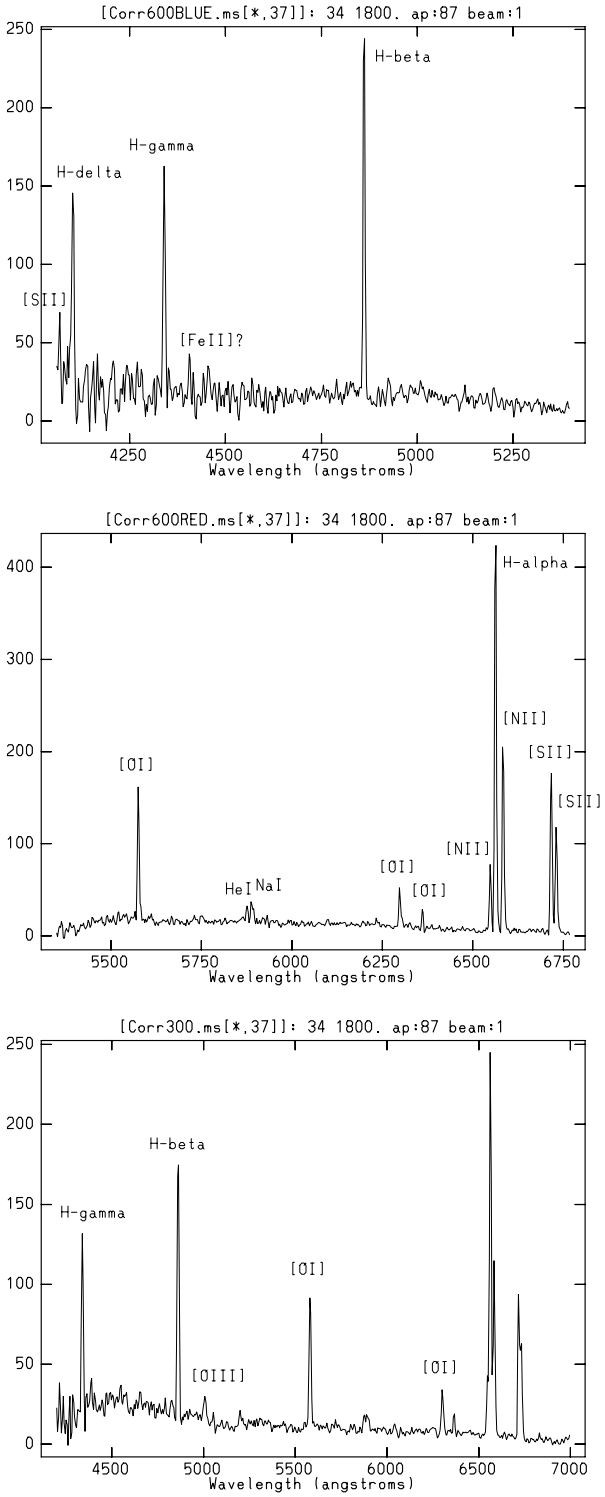

Figure 3.1: Three separate spectra of a bright filament in RCW 114. (RA (1950) = $17^{\rm h}\ 31^{\rm m}\ 39^{\rm s}$, Dec. (1950) = $-45^\circ\ 46'.6$). [S II]/Hα=0.69.

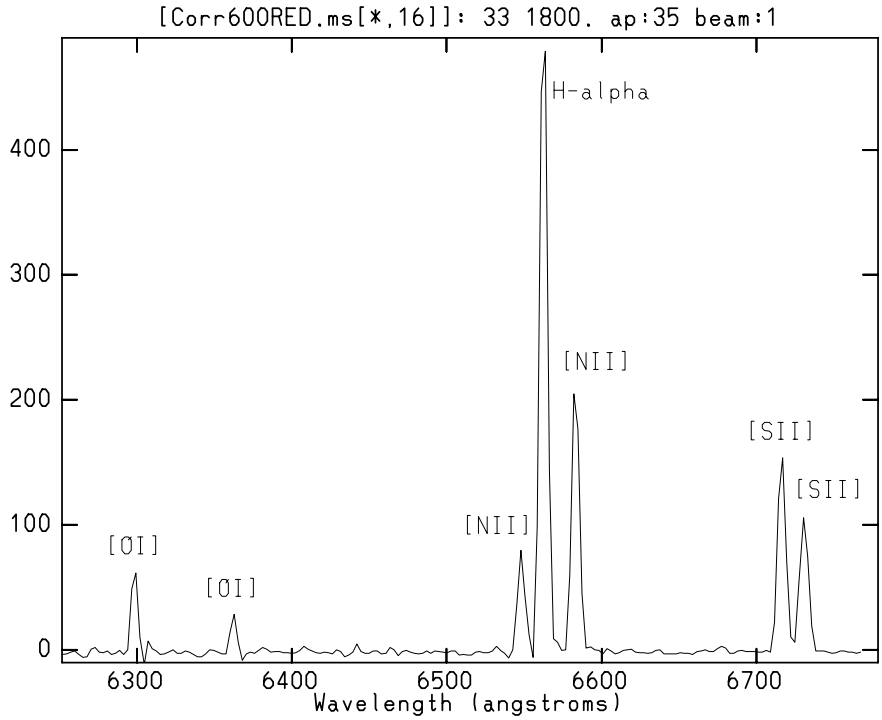

Figure 3.2: Enlarged red spectra of another filament at RA (1950) = $17^{\rm h}\ 30^{\rm m}\ 01^{\rm s}$, Dec. (1950) = $-46^\circ\ 11'.2$. Here [S II]/Hα=0.55.

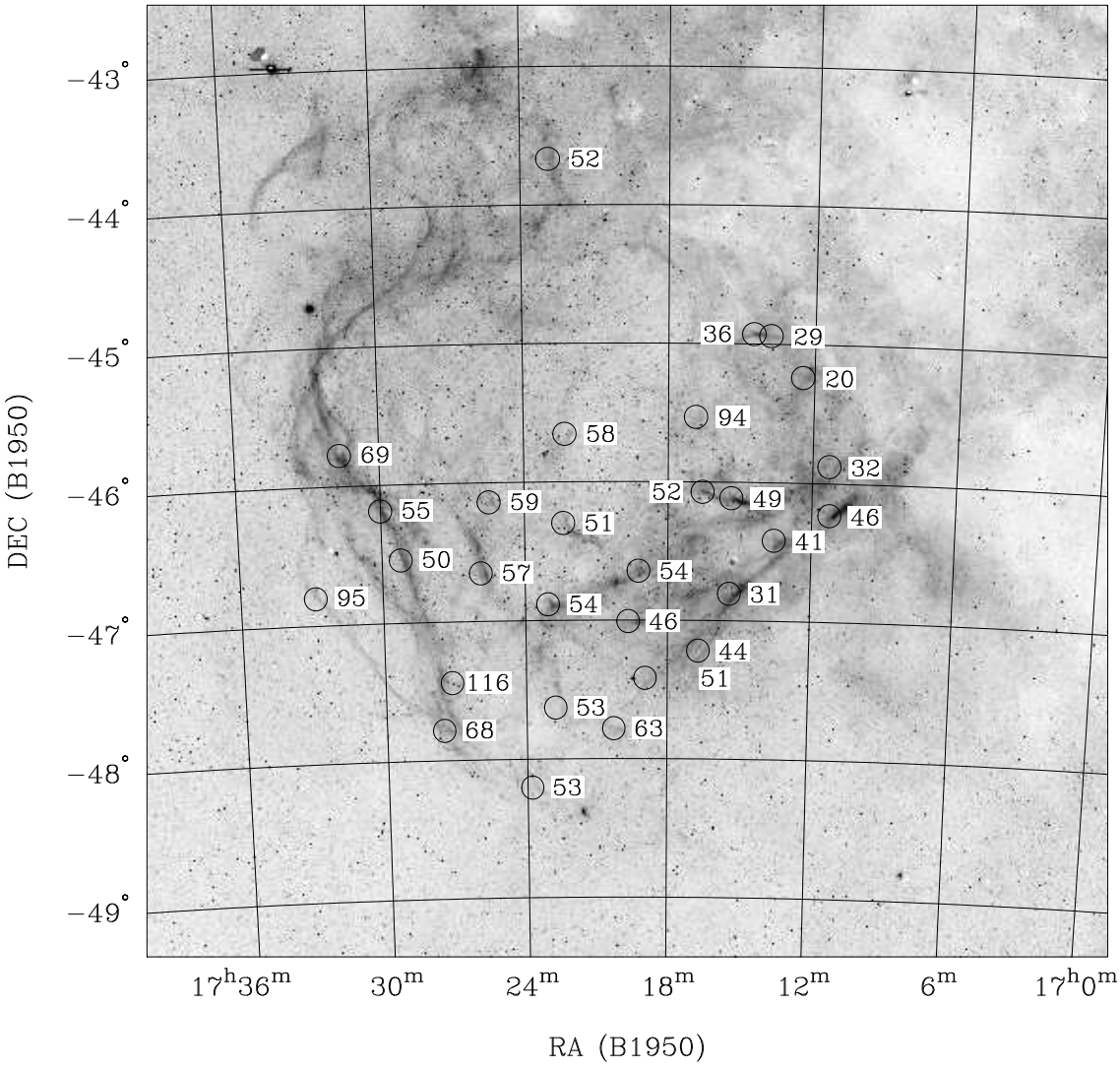

Figure 3.3: Plot of 100 × [S II]/Hα for the observed positions in RCW 114.

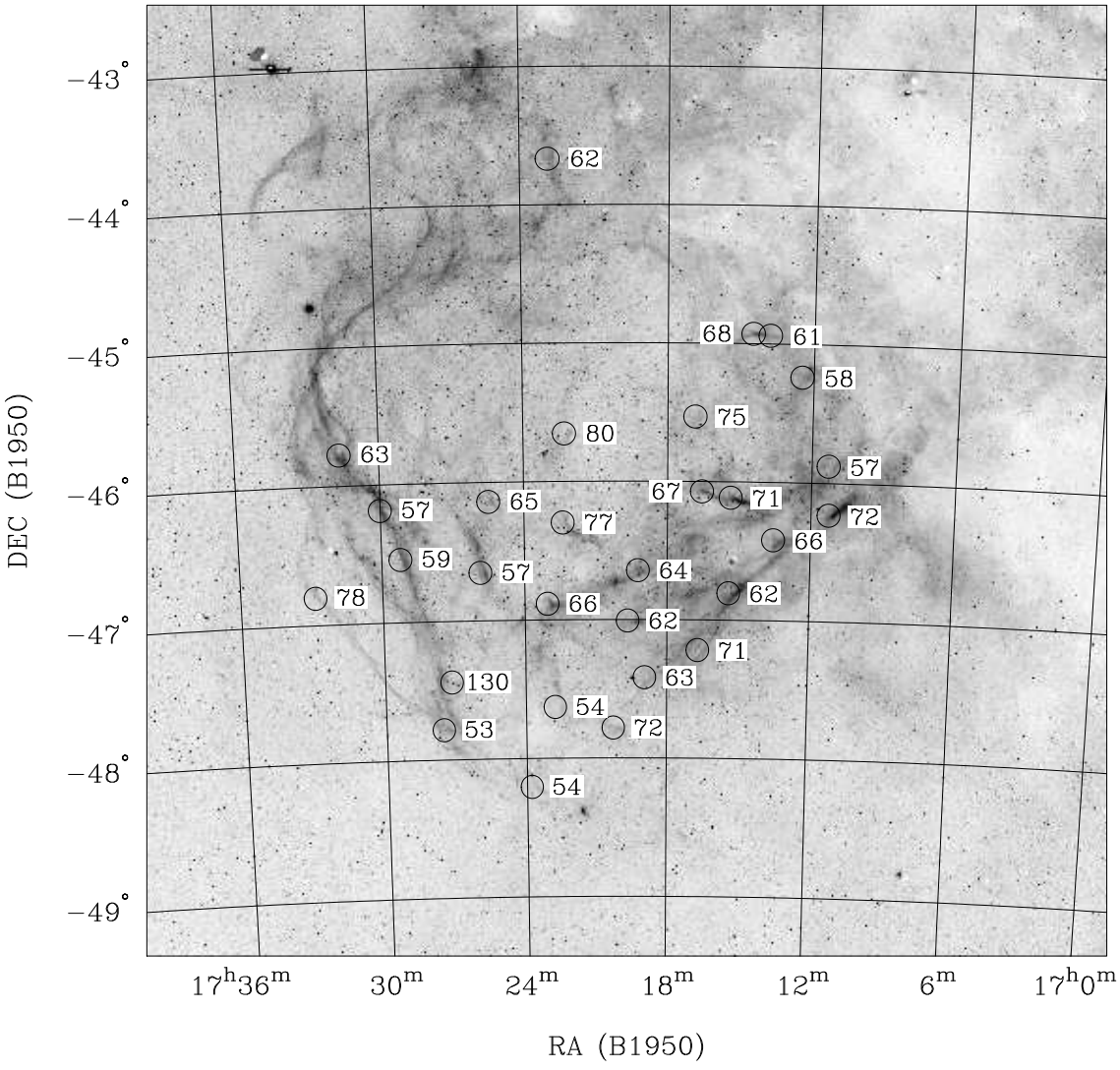

Figure 3.4: Plot of 100 × [N II]/Hα for the observed positions in RCW 114.

Chapter 4

A Survey of Optical Emission Associated With Galactic Supernova Remnants in the Southern Sky

4.1 Introduction

Supernova remnants (SNRs) are the signatures of violent explosions involving massive stars or white dwarfs. Both material ejected from the star and a shock wave interact with the surrounding interstellar medium, the effects of which can be observed in a wide variety of wavelength bands, primarily radio, optical and x-ray. These observations are useful for investigating the nature of progenitor stars, the rate and distribution of supernovae within galaxies, and the structure and composition of the surrounding interstellar medium (ISM).

As of 2000, 225 SNRs had been identified in radio emission within our galaxy, along with several other objects whose identity as an SNR is unclear (Green 2000). Of these 51 have associated optical emission. Of the 69 radio SNRs in the Northern sky, 31 have associated optical filaments. The higher proportion is due to the lower absorption away from the Galactic center. The first extensive catalogue of optical identifications was given in van den Bergh et al. (1973), where 24 SNRs were optically identified. Since then, further discoveries from radio and x-ray surveys, along with improved CCD imaging has doubled

the number of optical identifications in the galaxy. A summary of these objects is given in Table 4.1.

The surveys of van den Bergh et al. (1973) and of Zealey et al. (1979) used widefield images taken on red sensitive plates. The latter used ESO/SERC survey images which used IIIaF emulsion and an RG630 filter. Both of these surveys were limited by the high bandwidth being used, along with the sensitivity and resolution of the plates. They were also limited by the smaller number of Galactic SNRs then known, and the UKST southern red survey not being complete at the time of the Zealey et al. survey.

Our knowledge of the optical structure of SNRs is limited by:

- The large number of SNRs that have not been searched for optical emission
- Observations being limited in their ability to see deeply through the ISM
- Observations having insufficient resolution to see fine structures, or insufficient area coverage to see outlying features of SNRs
- Lack of observations in other optical lines, especially [O III] and [S II].

Our search using films from the AAO/UKST Galactic plane Hα Survey aims to address the first three of these points for SNRs in the southern sky.

4.2 The Hα Survey

The AAO/UKST Hα survey began in July 1997 and was completed by the end of 2003. A total of 233 field centres with 4° separation cover the southern Galactic plane to $|b| \leq 10°$, and 40 more cover the Magellanic Clouds. Each exposure images $6.^{\circ}5 \times 6.^{\circ}5$ of sky, however the filter provides optimal response within a circular diameter of 5.5°. A 15 minute red continuum exposure on Tech Pan film was also obtained for each field centre, normally directly after the Hα exposure.

Each 3 hour Hα exposure is obtained using a 356×356mm glass interference filter (Parker & Bland-Hawthorn 1998) which has a central wavelength of 6590 Å and a FWHM bandpass of 70 Å. They are taken on Tech Pan film (Parker & Malin 1999). In comparison with previous UKST R-band surveys on

IIIaF emulsion, Tech Pan film gives much improved sensitivity at this wavelength and resolution. Further details of the survey are given in Parker & Phillips (1998).

4.3 Film Search

From the catalogue of Green (2000), we selected for our search all southern supernova remnants with $|b| \leq 10^{\circ}$. Three high latitude objects do not lie on any of the survey fields, G296.5+10.0, G327.6+14.6 and G330.0+15.0. Non-survey Hα observations were made of these.

In total, 156 Galactic SNR in Green's catalogue form the basis of this search. Of these, 20 objects have been previously optically detected, namely those in table 4.1 from G4.5+6.8 to G13.3-1.3 inclusive, and from G260.4-3.4 to G340.6+0.3 inclusive. These objects allow a useful comparison to be made with the depth and amount of detail seen in previous film and CCD surveys.

The x-y position of the radio center of each remnant on the films is obtained using the UKST program PLADAT. In addition printed images of the field around each SNR are obtained using the STScI Digitized Sky Survey to ensure the correct area is being searched. As films become available containing SNR, the positions of any SNR in the field are identified. Using a wide angle magnifying lens, the field is then closely examined for any optical emission out to a radius greater than the radio size of the remnant.

As described in Walker et al. (2001), digitized images are obtained with a desktop scanner for interesting objects, and a coordinate system is then attached to these images using the KARMA program (Gooch 1996) to obtain accurate positions of new features.

To obtain better quality images of newly optically identified SNR, observing time was obtained at Mount Stromlo's 40 inch telescope at Siding Spring observatory. However due to bad weather little data was obtained, the best being for G296.8-0.3 as described below.

4.3.1 Supercosmos

Films obtained for the Hα survey are sent to the Royal Observatory, Edinburgh, for archival purposes and to be digitised with the high-precision mi-

crodensitometer SuperCOSMOS (Miller at al. 1992, Hambly et al. 1998). Films are scanned at a resolution of 10μm using a 2048 pixel linear CCD camera in about 2 hours for a full 14 inch Schmidt field.

For this project we applied to have fields containing known or newly identified optical SNR scanned as a priority. The data for each field is in FITS format as a grid of 4×4 2D images. Each sub-field is 7412 pixels square and has an overlap of 500 pixels with its neighbours. For larger objects these are combined using the IMCOMBINE procedure in IRAF. Coordinates are attached to extracted images using KARMA.

Subsequent to the completion of this film search, digitised data from this survey was made available over the internet, at the SuperCOSMOS H-alpha Survey (SHS) website, http://www-wfau.roe.ac.uk/sss/halpha/ .

4.4 New Optical Identifications

In Table 4.2 we present a list of the 86 SNRs that we have examined so far. We have indicated in the fourth column those that have been previously detected optically, and in the fifth column any objects that have been detected in this search. For objects not previously seen optically, an asterisk indicates that we are confident the emission is associated with the SNR, based on its coincidence with the radio source and the amount of filamentary emission seen. Objects with a question mark indicate that the association is very tentative, based on a very small amount of emission being seen and/or the emission lying outside the known bound of radio emission. 14 of the SNRs in Table 4.2 have been previously seen optically. Of these we have seen Hα filaments in all but 2. We have identified 8 SNR as having likely new optical identifications, and 4 as having possible new optical identifications.

4.4.1 Likely identifications

G4.2-3.5

First discovered in a survey by Reich et al. (1988,1990) with the Effelsberg 100-m telescope, G4.2-3.5 has a shell structure 28′ in diameter with a flux of 3.2 Jy at 1 GHz and an uncertain spectral index of $\alpha = -0.6$.

In Figure 4.1 we show an image of a filament just over $1'$ in length centered on $18^{\rm h}09^{\rm m}23^{\rm s}$ $-27°59.5'$ (J2000). Comparison with both the Effelsberg maps and the Parkes-MIT-NRAO 4850 MHz survey (Griffith & Wright 1993) show that this filament corresponds with enhanced radio emission on the North East edge of the remnant.

G32.8-0.1 (Kes 78)

An elongated shell with dimensions of approximately $10' \times 20'$, this object first appears as an SNR in the catalogues of Milne (1970) and Downes (1971). In the latter, the given position is close to the source G33.1-0.1 which is believed to be thermal (Caswell & Clark 1975), indicating confusion problems. Koralesky et al. (1998) detected OH (1720 MHz) maser emission on the east edge of the remnant with $V_{\rm LSR} = +86.1$ km s^{-1}.

We show in Figure 4.2 an image of this region from the Hα survey. This shows a near complete optical shell which matches in size and position radio structures seen by Koralesky et al. (1998). Towards the southern edge the emission has a very filamentary appearance. Elsewhere the emission is more diffuse, however finer structure may appear with deeper imaging. The optical emission appears weaker along the western edge of the shell, as does the radio emission.

Below this we have overlaid the Hα image with radio contours from a 1.7 GHz image supplied by Miller Goss based on VLA data obtained in December 1997 and February 1998. This data was also used for the image in Koralesky et al. (1998). In the southern half of the remnant, there is an excellent correspondence between the optical and radio, which shows that they are tracing the same shock structure. In the northern half, the radio emission is broader and less resolved. This corresponds to a more complex structure in the optical, with multiple filamentary structures visible in a radial direction from the centre. It is interesting to note than in the North-West corner, part of the shock has escaped into a less dense or cloud free region of the ISM. This is visible as faint optical emission extending in an arc towards $8^{\rm h}51^{\rm m}0^{\rm s}$ $-0°00'$ (J2000) which seems to correspond well with the large radio structure seen here. Also, one of the clouds with which this remnant is possibly interacting is visible as a region of obscuration at $8^{\rm h}51^{\rm m}45^{\rm s}$

$-0°00'$ (J2000). Further optical and radio studies would be useful to establish the excitation processes occurring here and the distance to the remnant.

G261.9+5.5

Also known as MSH 09-32 (Mills et al. 1960). Observations with the Parkes 64-m radio telescope (Hill 1967) showed it to be a supernova remnant by its non-thermal spectrum and shell structure. Higher resolution radio observations have been made with MOST (Kesteven & Caswell, 1987). Their image shows that the surface brightness is close to uniform across the remnant's area, with little evidence of any brightening towards the remnant's edge, or other structure such as filaments.

Colomb & Dubner (1980) detected clouds of neutral hydrogen associated with the remnant. In addition a deep Hα exposure showed a peak in optical emission inside the radio continuum emission.

Our image from the Hα survey (Figure 4.3) shows the presence of diffuse optical emission, with clearly defined boundaries on some sides but no filamentary structure. By overlaying with the PMN radio contours, it can be seen that the main body of the optical nebula overlays the radio shell, while the tailing emission to the west has no apparent radio counterpart.

G279.0+1.1

This remnant consists of a faint, incomplete shell structure $95'$ in diameter. It was discovered with the Hartesbeesthoek 26-m telescope (Woermann & Jonas 1988).

Observations with the Parkes radio telescope (Duncan et al. 1995) clearly show the shell structure of the SNR, and the large degree of polarization across the remnant. They also suggest the bright source G278.0+0.8 on the western limb to be extragalactic. Sub-arcminute resolution mapping has also been made of part of the remnant (Whiteoak & Green 1996).

Optically, we have detected a number of individual filaments probably associated with this remnant. The brightest of these, shown in Figure 4.4, has a double arc structure extending over $10'$ in declination. Close examination shows a faint extension towards $10^{\rm h}06^{\rm m}17^{\rm s}$ $-52°40'$ (J2000) and also a possible extension

to the south along RA=$10^{\rm h}06.0^{\rm m}$ (J2000). Comparison with the Duncan et al. maps show that this filament lies just outside the north-eastern radio limb.

We have also detected a network of small and faint filaments in the southern section of the remnant. The positions of these and the previously mentioned filament is given in Table 4.8. On the 843 MHz image of Whiteoak & Green, there is a faint radio filament extending through this area, most evident near $10^{\rm h}00.5^{\rm m}$ $-54°08'$ (J2000).

G286.5-1.2

The region surrounding this remnant contains some optical filaments that may be associated with it. However, their proximity to the Eta Carinae nebulosity must be carefully checked. $2' - 3'$ to the west of the 5th magnitude star HD 92063 we have detected two optical filaments in the UKST Hα Survey. These both run roughly from north to south and are almost completely in the area bound by RA = $10^{\rm h}35.6^{\rm m}$ to $10^{\rm h}36.2^{\rm m}$ (J2000), Dec. = $-59°30'$ to $-59°38'$ (J2000).

Further filaments are also visible to the south-west of these, especially at the locations $10^{\rm h}34.3^{\rm m}$ $-59°42'$ (J2000) and $10^{\rm h}34.8^{\rm m}$ $-59°45'$ (J2000).

At the time of writing we have not obtained a SuperCOSMOS scan of this area. Fortunately the filaments are visible on a red Digitized Sky Survey image. Comparison with an image from the MOST survey shows that both of the main southern optical filaments correspond well with the two southern ridges of radio emission. The longer filaments near HD 92063 correspond with a broader area of radio emission and lead down into the two radio ridges. This gives credence to their being a real association with the radio remnant.

G296.8-0.3 (1156-52)

G296.8-0.3 was identified as a supernova remnant by Large & Vaughan (1972). Observations at 408 MHz with the Molongolo Cross showed its extended structure and non-thermal spectral index $\alpha = -0.7 \pm 0.2$. They also investigated the possibility of it being associated with the nearby pulsar PSR 1154-62, however this was considered unlikely (Gaensler et al. 1998).

Subarcminute resolution radio images of this remnant have been made

by Whiteoak & Green (1996) at 843 MHz using MOST, and by Gaensler et al. (1998) at 1.344 GHz using the Australia Telescope Compact Array (ATCA). Both show a similar shell structure, with brightening on the south-east, south-west and north-west edges.

A 4σ x-ray detection of this remnant was made by Hwang & Markert (1994) using the ROSAT Position Sensitive Proportional Counter.

An image from the Hα survey revealed the presence of a faint filament to the north-west of the remnant's radio centre. Deeper Hα images were obtained in April 1998 using the 40″ telescope at Siding Spring Observatory, using a SITe 2K 2048×2048 CCD with a 20′.8 field of view at f/8. A 15Å Hα filter was used.

The image shown in Figure 4.5 is a composite of three 10 minute Hα exposures, which has been cropped to show details in the north-west section of the remnant. This has been overlaid with radio contours from Gaensler et al. (1998) with a resolution of $24''.3 \times 22''.4$, PA 14° in the figure below. Enlarged views of the western rim are shown in Figure 4.6.

A series of at least three optical filaments are visible, brightest to the north. These extend to the south-west for at least $6' - 7'$. Comparison with the ATCA image shows that optical emission can be associated with the brightest, outermost shock, and with the ridge extending east of this at declination $-62°31'$ (J2000). The most easterly of the three long optical filaments also appears to be associated with a radio filament, clearest in the Gaensler et al. image, which passes through $11^{\rm h}58.0^{\rm m}$ $-62°34'$ (J2000).

G315.4-0.3

A 408 MHz survey of the Southern Galactic Plane with the Molongolo radio telescope identified 28 new galactic supernova remnants, including G315.4-0.3 (Clark et al. 1973, 1975). Higher resolution observations by Caswell et al. (1981) at 1415 MHz using the Fleurs synthesis telescope, and at 843 MHz with MOST (Whiteoak & Green 1996), show it to consist of a weak shell structure, approximately $24' \times 13'$ in size in the latter survey. They also show 2 compact sources dominating the field, G315.31-0.27, a flat spectrum HII region, and G315.59-0.21, a steep spectrum source which is possibly extragalactic.

Our image from the UKST Hα survey shows the presence of three dis-

tinct optical filaments within the region of the radio emission (Figure 4.7). To the east of the radio centre, filaments are located at $14^{\rm h}36.7^{\rm m}$ $-60°31'$ (J2000) and at $14^{\rm h}36.5^{\rm m}$ $-60°33'$ (J2000) which are north-south in orientation and approximately $3'$ and $2'$ in length respectively. The filament to the west of centre, located at $14^{\rm h}35.2^{\rm m}$ $-60°33'$ (J2000), is $2'-3'$ in length and roughly north-west to south-east in orientation. All of these are surrounded by diffuse background emission, and there is evidence of fainter filamentary structure in the area, especially near the eastern pair.

Comparison with radio contours from the MOST survey (figure below) shows that the easternmost optical filament can be associated with a ridge of radio emission, best seen in the greyscale image of Whiteoak & Green (1996). Better observations are needed to establish the true radio extent of the remnant and how the optical filaments relate to this structure.

G340.4+0.4

This supernova remnant was discovered in the same survey as G315.4-0.3 (Clark et al. 1973, 1975). Caswell et al. (1983) mapped the remnant at 1415 MHz using the Fleurs synthesis telescope showing a clear shell structure. This was improved on by Dubner et al. (1996), whose maps at 330 MHz and 1425 MHz using the VLA show the remnant to be elongated in the east-west direction, with multiple filamentary structures visible. Hints of this structure are also visible in the 843 MHz maps of Whiteoak & Green (1996) obtained with MOST.

In Figure 4.8 we show an optical image of the region from the UKST Hα Survey, which has been overlaid with contours from the MOST survey in the figure below. The optical image shows the presence of the globule Barnard 235 at the top of the image. There is also a partial ring of absorbing material which spatially corresponds with the southern edge of the radio shell, but extends further outwards on the eastern and western sides. This may indicate that the remnant extends further outwards than has been seen in the radio, it would be necessary to investigate neutral hydrogen gas surrounding the remnant to establish this.

On the northern rim of the radio shell, we have discovered a faint optical

filament extending from approximately $16^{\rm h}46.9^{\rm m}$ $-44°34'$ (J2000) to $16^{\rm h}46.6^{\rm m}$ $-44°37'$ (J2000) and lying nearly perpendicular to the edge of the radio shell. This and the closely spaced radio contours suggest the remnant is interacting with a cloud on its northern edge. It is also possible that the optical filament is unrelated to G340.4+0.4, and perhaps associated with filaments to the north-west of Barnard 235 (Walker & Zealey 2001).

4.4.2 Possible identifications

G308.8-0.1/G309.2-0.6

A small patch of optical emission is visible at $13^{\rm h}44.5^{\rm m}$ $-62°47'$. This lies midway between these two remnants, which are separated by $42'$. From the Σ-D relation of Case & Battacharya (1998) these two remnants have estimated distances of 16.8 kpc and 8.0 kpc respectively, indicating an association with the latter is more likely but still very uncertain.

G309.8+0.0

A small patch of optical emission under $1'$ in size is visible in both the Hα survey and DSS red images at $13^{\rm h}51^{\rm m}37^{\rm s}$ $-61°39.7'$ (J2000). This is $10' - 15'$ north of the extent of radio emission visible in the MOST survey for this remnant, making an association a low possibility. This emission is also very close to the thermal radio source PMN J1350-6141.

G315.9-0.0/G316.3-0.0 (MSH 14-57)

An oddly shaped optical filament is located between these two remnants and could be associated with either of them. The southern component is centred on $14^{\rm h}37^{\rm m}52^{\rm s}$ $-59°49.9'$ (J2000) and is between $20'$ and $30'$ in length. The northern component is at $14^{\rm h}37^{\rm m}55^{\rm s}$ $-59°49.3'$ (J2000) and is $10'$ to $15'$ in length. Both appear to be joined by fainter emission.

G322.5-0.1

On an Hα survey image of this field, a small optical patch under $10''$ in size, which appears fainter on a red DSS image, can be seen at $15^{\rm h}23^{\rm m}23^{\rm s}$

$-57°10.8'$ (J2000). Comparison with an image from the MOST survey shows that this coincides very well with a peak in the 843 MHz radio flux just north of the remnant's southern edge. Whiteoak (1992) estimates a distance of ~ 5 kpc, which is compatible with optical emission being visible.

4.5 The Coalsack Loop

The Coalsack Loop is a large ring of Hα emitting nebulosity surrounding the Coalsack Nebula, about 10° in diameter. It was first noticed on ESO/SERC Sky Survey plates, though it is only partly visible and very faint. During February 1997, this region was imaged using the 16-inch telescope at Siding Spring Observatory. The telescope had been greatly modified for the Mount Stromlo CCD survey described by Buxton, Bessell & Watson (1998). Images covering 7° of sky were obtained using a 400mm f/4.5 lens in front of a 2k × 2k CCD, which replaced the original mirror and tubing.

The image shown in Figure 4.9 is a composite of four fields, each being a 15 minute exposure through a 15$\mathring{A}$ Hα filter and using standard ESO/SERC Sky Survey field centres. Each image was flat field corrected, and had bias and dark frames subtracted using standard IRAF procedures. On these images the loop is visible over about three-quarters of a circle. [S II] images have shown this emission to be weak.

In Figure 4.10 we present an image of the same region from The Southern H-Alpha Sky Survey Atlas (SHASSA) (Gaustad et al. 2001), centred on $12^{h}57^{m}35^{s}$ $-61°20'$ (J 2000) and is about 13° in size. This survey imaged the southern Galactic plane with a robotic camera operating at Cerro Tololo Inter-American Observatory (CTIO) in Chile. Each image was obtained with a 52 mm f/1.6 Canon lens giving a scale of $47''.64$ pixel^{-1}. The Hα filter had a bandwidth of 3.2 nm. This downloaded imaged had been smoothed to a resolution of 4.0 arcmin, to remove most star images and better show the underlying emission. It can be seen that there is an excellent agreement of the structure in both images, and that a lot more faint filamentary structure is visible in the SHASSA image. Images from the AAO/UKST Hα Survey further confirm the presence of these filaments and have shown many of them to be on the order of arcseconds or less in width.

This object is most likely the expanding remains of an old supernova

remnant or HII region, and its location suggests that it may be interacting with the Coalsack. Further observations will be necessary to examine these possibilities, most importantly determining the object's distance. The Coalsack is composed of two clouds located at distances of 188 pc and 243 pc (Seidensticker & Schmidt-Kaler 1989). Adopting an angular size of 10° gives a diameter of 33 pc or 43 pc respectively if the Coalsack Loop is interacting with either cloud.

The Coalsack Loop has been identified as G303.5+0 in the radio continuum survey of Duncan et al. (1995). Here a near complete shell structure is visible. It is also clearly visible in images from the PMN 4850 MHz survey (Griffith & Wright 1993). These surveys show the presence of several large shell structures along the Galactic plane.

McClure-Griffiths et al. (2001) imaged the Coalsack region in HI emission as part of the Southern Galactic Plane Survey with the Parkes Radio Telescope. They identified a shell GSH 305+01-24, with an angular size of $7° \times 11°$, which is positionally coincident with the Coalsack Loop. They detect infrared emission from the shell, suggest that the emission is thermal and from the shell rather than an SNR, and that its expansion has been powered by stellar winds of the Centaurus OB1 association. A distance of about 2.2 kpc is derived along with dimensions of 280×240 pc.

4.6 Discussion

The objects we have identified in this paper with possible optical associations are widely varied in both their morphologies and in how they relate to the radio remnant. G32.8-0.1 shows an almost optical complete shell, while the others have one or more filaments or a diffuse structure such as with G261.9+5.5. The correspondence of the optical and radio emission also varies from very good to poor, however in some of these cases better correspondence may be seen with more sensitive or higher resolution radio maps. A summary of the new associations and their correspondence with the radio remnant is given in Table 4.4.

An immediate consequence of optical identification of these supernova remnants is that their distance must be relatively close within the galaxy. Despite their distances being fairly uncertain, almost all presently known optical SNR in the galaxy should lie within 5-6 kpc of the Earth (e.g. Case & Bhattacharya

1998). We have given best estimates from this paper of the distances to our likely new optical associations in Table 4.4. All of these are based on their Σ-D relationship except for G315.4-0.3. Despite the errors being estimated at 40% for any individual remnant, and problems with the relation itself (Green 1984,1991) this clearly shows that with the Hα survey we are detecting SNR beyond 5 kpc distance and possibly as far as 10 kpc. Distances to our possible optical SNR associations, as given above, mostly lie within this range, and so cannot be ruled out on this basis.

4.7 Conclusion

Using films from the UKST Hα Survey we have examined the locations of 86 Galactic supernova remnants for optical emission. From these we have likely detections of 8 objects and possible detections of 4 others. The new optical features show a variety of morphologies and are varied in their relationship to the remnants' radio emission. Distance estimates to these SNR, while having a large error, indicate that we may be detecting optical features out to a distance of 10 kpc, a direct result of the improved spatial resolution and sensitivity of the film in comparison with previous optical surveys.

4.8 Acknowledgements

We would like to thank Miller Goss and Brian Gaensler for supplying the radio images of G32.8-0.1 and G296.8-0.3 respectively. The Digitized Sky Surveys were produced at the Space Telescope Science Institute under U.S. Government grant NAG W-2166 based on photographic data obtained using the Orsin Schmidt Telescope on Palomar Mountain and the UK Schmidt Telescope. The UK Schmidt Telescope was operated by the Royal Observatory Edinburgh, with funding from the UK Science and Engineering Research Council until 1988 June, and thereafter by the Anglo-Australian Observatory. The MOST is operated by the University of Sydney with support from the Australian Research Council and the Science Foundation for Physics within the University of Sydney. The image shown in Figure 4.10 is from the Southern H-Alpha Sky Survey Atlas (SHASSA), which is supported by the National Science Foundation.

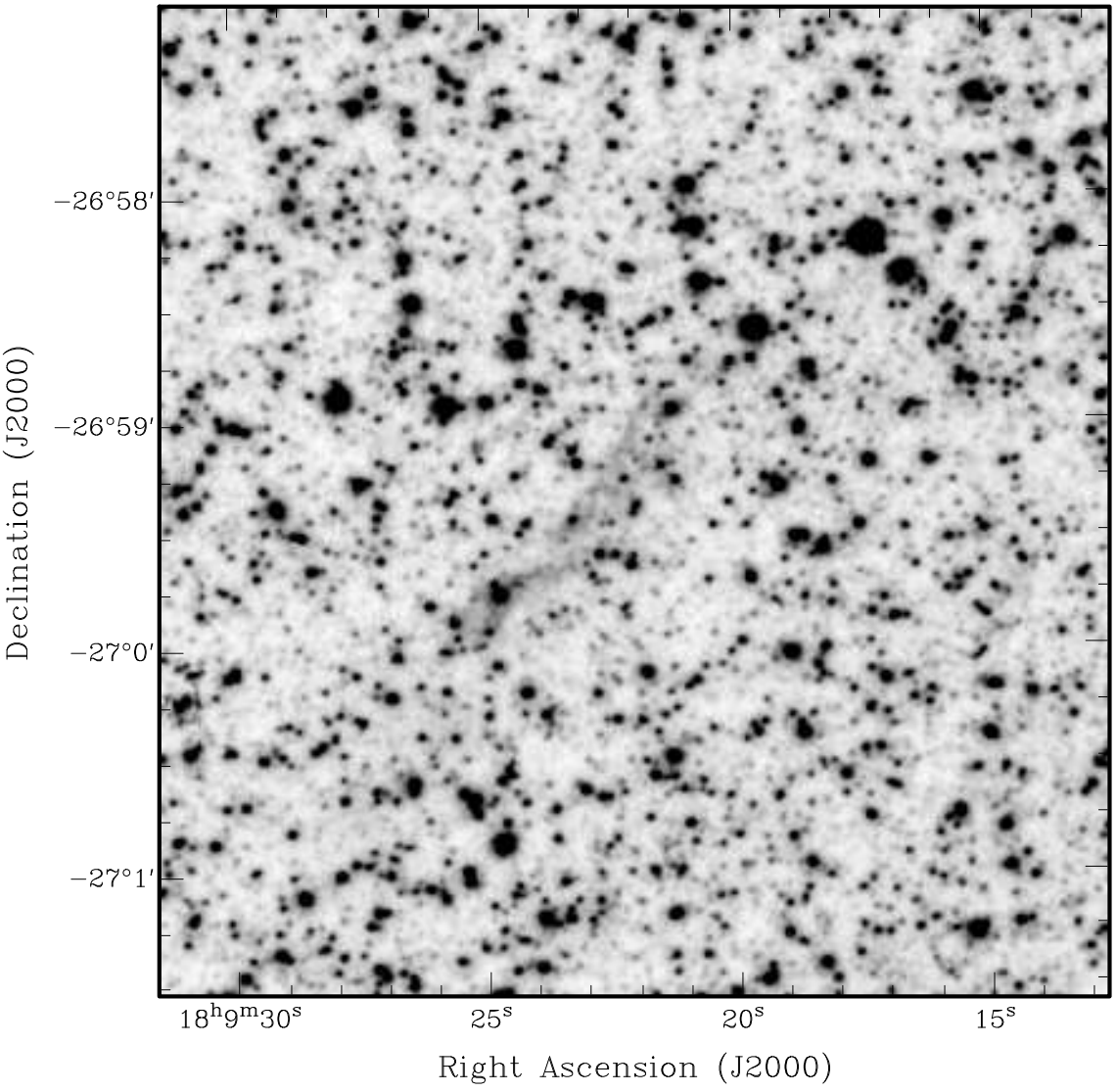

Figure 4.1: Hα image of G4.2-3.5

Table 4.1: Optical Galactic SNR

Catalogue Designation	Other Names	Discovery Reference
G4.5+6.8	Kepler, SN1604, 3C 358	1
G5.4-1.2	Milne 56	2
G6.4-0.1	W28	3
G13.3-1.3		4
G31.5-0.6		5
G34.7-0.4	W44, 3C 392	6
G39.7-2.0	W50, SS433	7,8
G53.6-2.2	3C400.2, NRAO 611, HC 42	9
G65.3+5.7		10
G67.7+1.8		5
G69.0+2.7	CTB 80	11
G73.9+0.9		12?
G74.0-8.5	Cygnus Loop, Veil Nebula	
G78.2+2.1	DR4, gamma Cygni, W66	13
G82.2+5.3	W63	14
G89.0+4.7	HB 21	15
G109.1-1.0	CTB 109	16
G111.7-2.1	Cassiopeia A, 3C 461	17
G114.3+0.3		18
G116.5+1.1		18
G116.9+0.2	CTB 1	3
G119.5+10.2	CTA 1	19
G120.1+1.4	Tycho, 3C 10, SN1572	20,21
G126.2+1.6		22
G127.1+0.5	R5	23
G130.7+3.1	3C58, SN1181	24
G132.7+1.3	HB 3, CTA 2	9?
G160.9+2.6	HB 9, CTA 33	25
G166.0+4.3	VRO 42.05.01	
G166.2+2.5	OA 184	
G180.0-1.7	S147	
G184.6-5.8	Crab Nebula, 3C 144, SN1054	
G189.1+3.0	IC443, 3C 157	
G192.8-1.1	PKS 0607+17	
G205.5+0.5	Monoceros Nebula, Downes 14	26
G206.9+2.3	PKS 0646+06	
G211.7-1.1		
G260.4-3.4	Puppis A, MSH 08-44	17
G263.9-3.3	Vela (XYZ)	
G272.2-3.2		27
G284.3-1.8	MSH 10-53	9
G290.1-0.8	MSH 11-61A	28,29
G292.0+1.8	MSH 11-54	30

Table 4.1: Optical Galactic SNR cont.

Catalogue Designation	Other Names	Optical Discovery Reference
G296.1-0.5		31
G296.5+10.0	PKS 1209-51/52	32
G299.2-2.9		33
G315.4-2.3	RCW 86, MSH 14-63, PKS 1439-62	
G320.4-1.2	MSH 15-52, RCW 89, Kes 23	
G326.3-1.8	MSH 15-56	34,2
G327.6+14.6	SN1006, PKS 1459-41	35
G332.4-0.4	RCW 103, Kes 33, PKS 1613-50	
G338.1+0.4		2
G340.6+0.3		2

References: 1: Baade (1943), 2: Zealey et al. (1979), 3: van den Berg (1960), 4: Seward et al. (1995), 5: Mavromatakis et al. (2001), 6: Rho et al. (1994), 7: van den Berg (1980), 8: Zealey et al. (1980), 9: van den Bergh et al. (1973), 10: Gull et al. (1977), 11: Angerhofer et al. (1981), 12: Lozinskaya et al. (1993), 13: Drake (1959) 14: Sabbadin (1976), 15: Minkowski (1958), 16: Blair & Kirshner (1981), 17: Baade & Minkowski (1954), 18: Fesen et al. (1997), 19: Harris & Roberts (1960), 20: Minkowski (1954), 21: Minkowski (1959), 22: Blair et al. (1980), 23: Xilouris et al. (1993), 24: van den Berg (1978), 25: Hanbury Brown et al. (1954), 26: Morgan et al. (1955), 27: Greiner et al. (1994), 28: Elliot & Malin (1979), 29: Kirshner & Winkler (1979), 30: Goss et al. (1979), 31: Longmore et al. (1977), 32: Irvine & Irvine (1974), 33: Busser et al. (1996), 34: van den Berg (1979), 35: van den Bergh (1976)

Table 4.2: Supernova remnants examined for optical emission

Object	R.A. (J2000.0)	Dec. (J2000.0)	Prev. known optically	Seen here	Notes
G0.0+0.0	$17^h45^m44^s$	$-29°00'$	...	...	Sgr A East
G0.3+0.0	$17^h46^m15^s$	$-28°38'$	...	...	
G0.9+0.1	$17^h47^m21^s$	$-28°09'$	...	...	
G1.0-0.1	$17^h48^m30^s$	$-28°09'$	...	...	
G1.4-0.1	$17^h49^m39^s$	$-27°46'$	...	...	
G1.9+0.3	$17^h48^m45^s$	$-27°10'$	...	...	
G4.2-3.5	$18^h08^m55^s$	$-27°03'$	...	*	
G4.5+6.8	$17^h30^m42^s$	$-21°29'$	*	?	SN1604 (Kepler)
G6.4+4.0	$17^h45^m10^s$	$-21°22'$	...	...	
G13.3-1.3	$18^h19^m20^s$	$-18°00'$	*	*	
G30.7-2.0	$18^h54^m25^s$	$-02°54'$	...	...	
G31.5-0.6	$18^h51^m10^s$	$-01°31'$	...	...	
G32.0-4.9	$19^h06^m00^s$	$-03°00'$	...	...	3C396.1
G32.8-0.1	$18^h51^m25^s$	$-00°08'$	...	*	Kes 78
G33.2-0.6	$18^h53^m50^s$	$-00°02'$	...	...	
G261.9+5.5	$09^h04^m20^s$	$-38°42'$	...	*	MSH 09-32
G272.2-3.2	$09^h06^m50^s$	$-52°02'$	*	*	
G279.0+1.1	$09^h57^m40^s$	$-53°15'$	...	*	
G284.3-1.8	$10^h18^m15^s$	$-59°00'$	*	*	MSH 10-53
G286.5-1.2	$10^h35^m40^s$	$-59°42'$	...	?	
G289.7-0.3	$11^h01^m15^s$	$-60°18'$	...	...	
G290.1-0.8	$11^h03^m05^s$	$-60°56'$	*	?	MSH 11-61A
G291.0-0.1	$11^h11^m54^s$	$-60°38'$	...	...	(MSH 11-62)
G292.0+1.8	$11^h24^m36^s$	$-59°16'$	*	*	MSH 11-54
G293.8+0.6	$11^h35^m00^s$	$-60°54'$	...	...	
G294.1-0.0	$11^h36^m10^s$	$-61°38'$	...	...	
G296.1-0.5	$11^h51^m10^s$	$-62°34'$	*	*	
G296.8-0.3	$11^h58^m30^s$	$-62°35'$	...	*	1156-62
G298.5-0.3	$12^h12^m40^s$	$-62°52'$	...	...	
G298.6-0.0	$12^h13^m41^s$	$-62°37'$	...	...	
G299.2-2.9	$12^h15^m13^s$	$-65°30'$	*	*	
G299.6-0.5	$12^h21^m45^s$	$-63°09'$	...	...	
G301.4-1.0	$12^h37^m55^s$	$-63°49'$	...	...	
G302.3+0.7	$12^h45^m55^s$	$-62°08'$	...	...	
G304.6+0.1	$13^h05^m59^s$	$-62°42'$	...	...	Kes 17
G308.1-0.7	$13^h37^m37^s$	$-63°04'$	...	...	
G308.8-0.1	$13^h42^m30^s$	$-62°23'$	...	?	
G309.2-0.6	$13^h46^m31^s$	$-62°54'$	...	...	
G309.8+0.0	$13^h50^m30^s$	$-62°05'$	...	?	
G310.6-0.3	$13^h58^m00^s$	$-62°09'$	...	...	Kes 20B
G310.8-0.4	$14^h00^m00^s$	$-62°17'$	...	?	Kes 20A
G311.5-0.3	$14^h05^m38^s$	$-61°58'$	...	...	
G312.4-0.4	$14^h13^m00^s$	$-61°44'$	...	...	

Table 4.2: Supernova remnants examined for optical emission cont.

Object	R.A. (B1950.0)	Dec. (B1950.0)	Prev. known optically	Seen here	Notes
G315.4-2.3	$14^h43^m00^s$	$-62°30'$	*	*	RCW 86, MSH 14-63
G315.4-0.3	$14^h35^m55^s$	$-60°36'$	...	*	
G315.9-0.0	$14^h38^m25^s$	$-60°11'$	...	?	
G316.3-0.0	$14^h41^m30^s$	$-60°00'$	...	?	(MSH 14-57)
G317.3-0.2	$14^h49^m40^s$	$-59°46'$	...	...	
G318.2+0.1	$14^h54^m50^s$	$-59°04'$	...	...	
G318.9+0.4	$14^h58^m30^s$	$-58°29'$	...	...	
G320.4-1.2	$15^h14^m30^s$	$-59°08'$	*	*	RCW 89, MSH 15-52
G320.6-1.6	$15^h17^m50^s$	$-59°16'$	...	...	
G321.9-1.1	$15^h23^m45^s$	$-58°13'$	...	...	
G321.9-0.3	$15^h20^m40^s$	$-57°34'$	...	...	
G322.5-0.1	$15^h23^m23^s$	$-57°06'$	...	?	
G323.5+0.1	$15^h28^m42^s$	$-56°21'$	...	...	
G327.6+14.6	$15^h02^m50^s$	$-41°56'$	*	*	SN1006, PKS 1459-41
G328.4+0.2	$15^h55^m30^s$	$-53°17'$	...	...	(MSH 15-57)
G329.7+0.4	$16^h01^m20^s$	$-52°18'$	...	...	
G333.0+15.0	$15^h10^m00^s$	$-40°00'$	...	...	Lupus Loop
G330.2+1.0	$16^h01^m06^s$	$-51°34'$	...	...	
G332.0+0.2	$16^h13^m17^s$	$-50°53'$	...	...	
G332.4-0.4	$16^h17^m33^s$	$-51°02'$	*	*	RCW 103
G332.4+0.1	$16^h15^m17^s$	$-50°42'$	...	...	Kes 32, MSH 16-51
G338.1+0.4	$16^h37^m59^s$	$-46°24'$	*	*	
G340.4+0.4	$16^h46^m31^s$	$-44°39'$	...	*	
G340.6+0.3	$16^h47^m41^s$	$-44°34'$	*	*	
G341.2+0.9	$16^h47^m35^s$	$-43°47'$	...	...	
G341.9-0.3	$16^h55^m01^s$	$-44°01'$	...	...	In Kes 45 region
G342.0-0.2	$16^h54^m50^s$	$-43°53'$	...	...	In Kes 45 region
G342.1+0.9	$16^h50^m43^s$	$-43°04'$	...	...	
G343.1-2.3	$17^h08^m00^s$	$-44°16'$	...	...	
G343.1-0.7	$17^h00^m25^s$	$-43°14'$	...	...	
G344.7-0.1	$17^h03^m51^s$	$-41°42'$	...	...	
G345.7-0.2	$17^h07^m20^s$	$-40°53'$	...	...	
G346.6-0.2	$17^h10^m19^s$	$-40°11'$	...	...	
G348.5-0.0	$17^h15^m26^s$	$-38°28'$	...	...	
G348.5+0.1	$17^h14^m06^s$	$-38°32'$	...	...	CTB 37A
G348.7+0.3	$17^h13^m55^s$	$-38°11'$	...	...	CTB 37B
G349.2-0.1	$17^h17^m15^s$	$-38°04'$	...	...	
G354.1+0.1	$17^h30^m28^s$	$-33°46'$	...	...	
G354.8-0.8	$17^h36^m00^s$	$-33°42'$	...	...	
G355.6-0.0	$17^h35^m16^s$	$-32°38'$	...	...	
G356.3-0.3	$17^h37^m56^s$	$-32°16'$	...	...	
G359.1-0.5	$17^h45^m30^s$	$-29°57'$	...	...	
G359.1+0.9	$17^h39^m36^s$	$-29°11'$	...	...	

Table 4.3: Optical filaments in G279.0+1.1

Filament Number	R.A. (J2000.0)	Dec (J2000.0)
1	$10^{h}06^{m}12s$	$-52°48'$
2	$10^{h}00.1m$	$-53°44'$
3	$9^{h}57^{m}17s$	$-53°53'$
4	$9^{h}57^{m}52s$	$-53°41'$
5	$9^{h}59^{m}21s$	$-54°04.5'$
6	$9^{h}59^{m}45s$	$-54°02 - 06'$
7	$9^{h}56^{m}20s$	$-53°54'$

Table 4.4: Summary of new probable optical SNR associations

Catalogue Designation	Optical Features	Radio Correlation	Best Distanc Estimate (k
G4.2-3.5	Single filament	Matches enhanced radio emission on rim	9.8
G32.8-0.1	Almost complete shell	Very good	6.3
G261.9+5.5	Diffuse filled structure	Position and size match well	5.9
G279.0+1.1	Several filaments	Good	3.2
G286.5-1.2	Several filaments	Very good	15.1
G296.8-0.3	Several filaments	Very good	6.9
G315.4-0.3	Small filaments	Partial, interior to shell	7.2
G340.4+0.4	Single filament	Perpendicular and across shell rim	10.5

Distance estimates are from the revised Σ-D relation of Case & Bhattacharya (1998) except for G315.4-0.3 which is from Rosado et al. (1996).

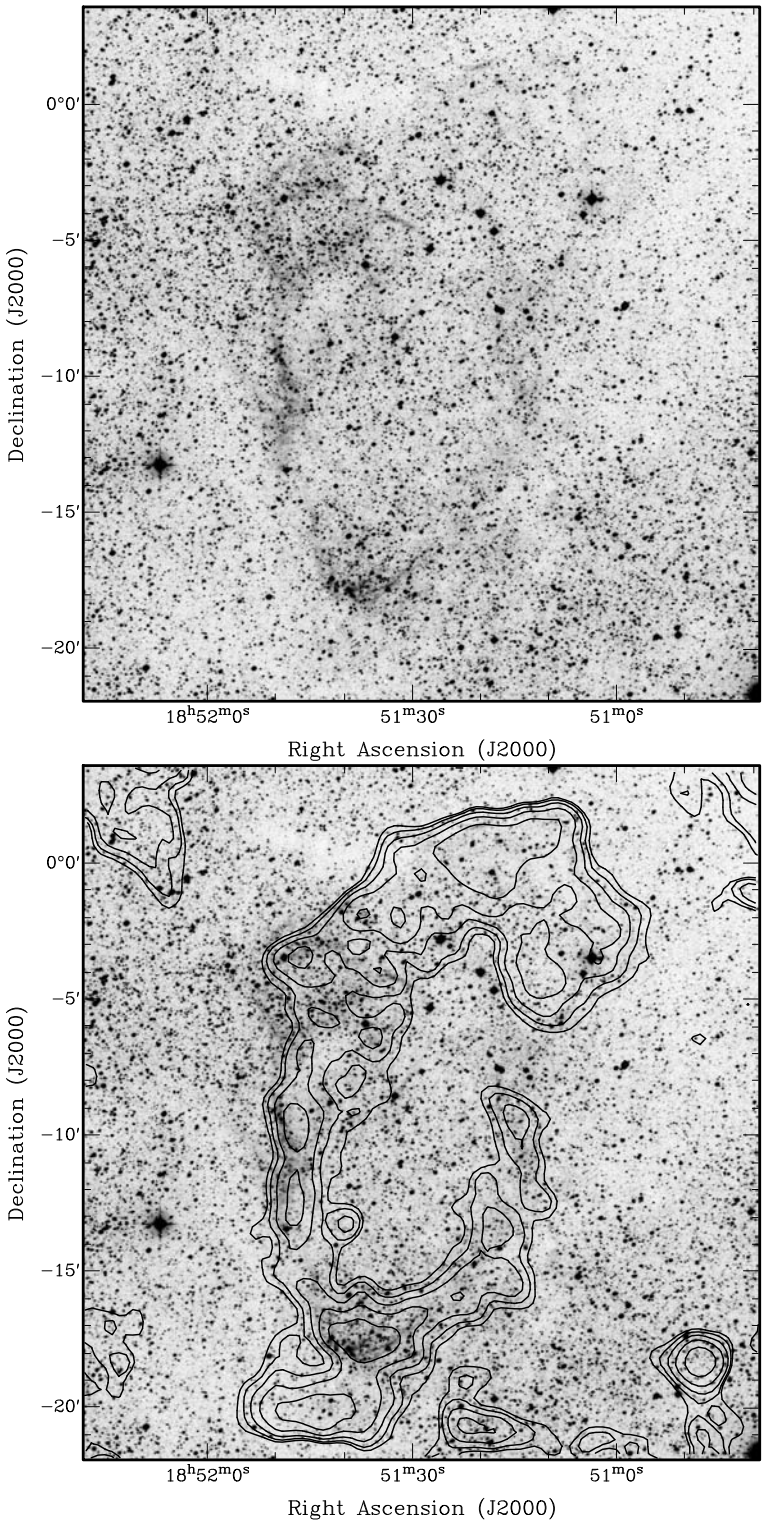

Figure 4.2: a) Hα image of G32.8-0.1. b) Hα image overlaid with VLA 1.7 GHZ image. Contours (mJy/beam) = 3,6,12,24,48. The beamsize is $56'' \times 43''$

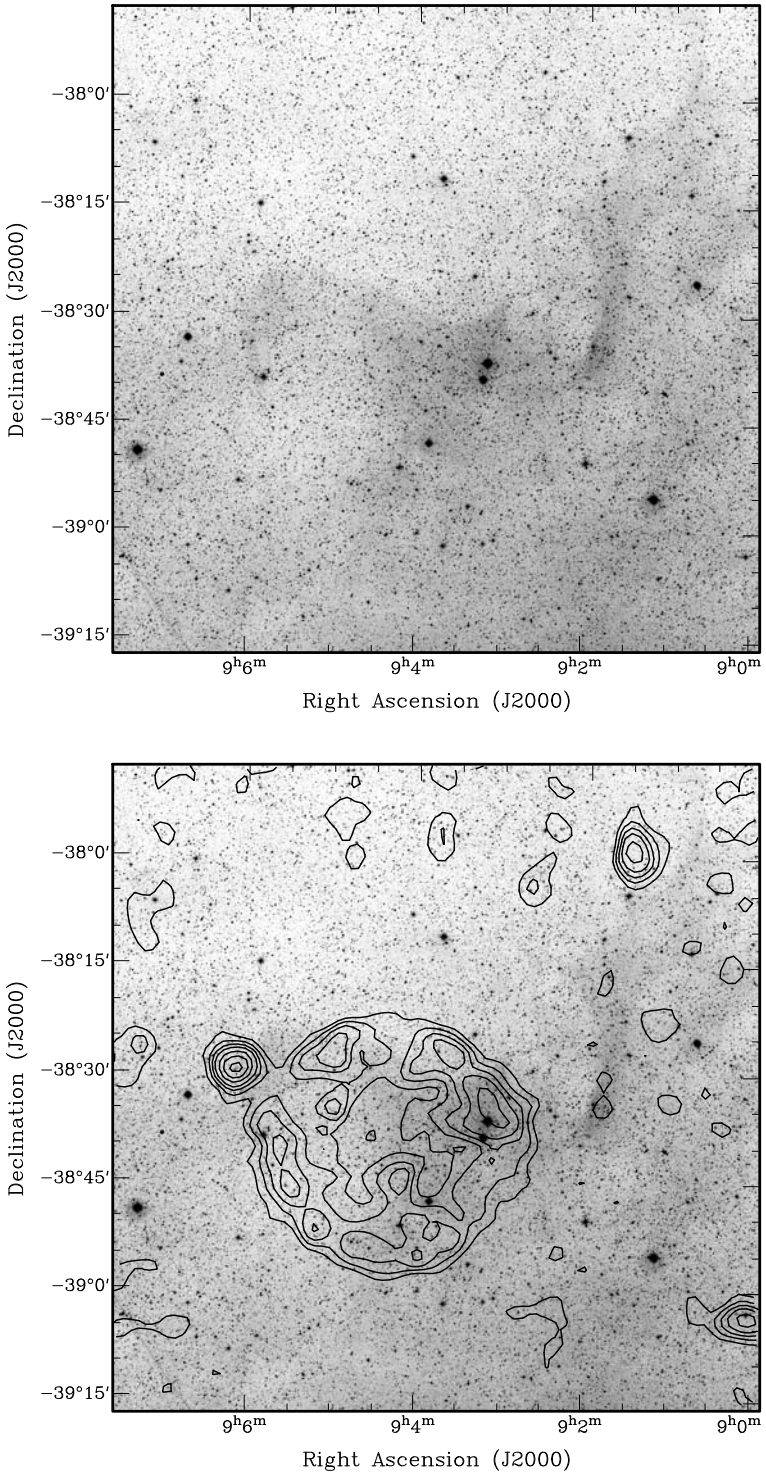

Figure 4.3: a) Hα image of G261.9+5.5. b) Hα image overlaid with PMN radio survey. Contours (mJy/beam) = 20,40,60,80,110,140,170

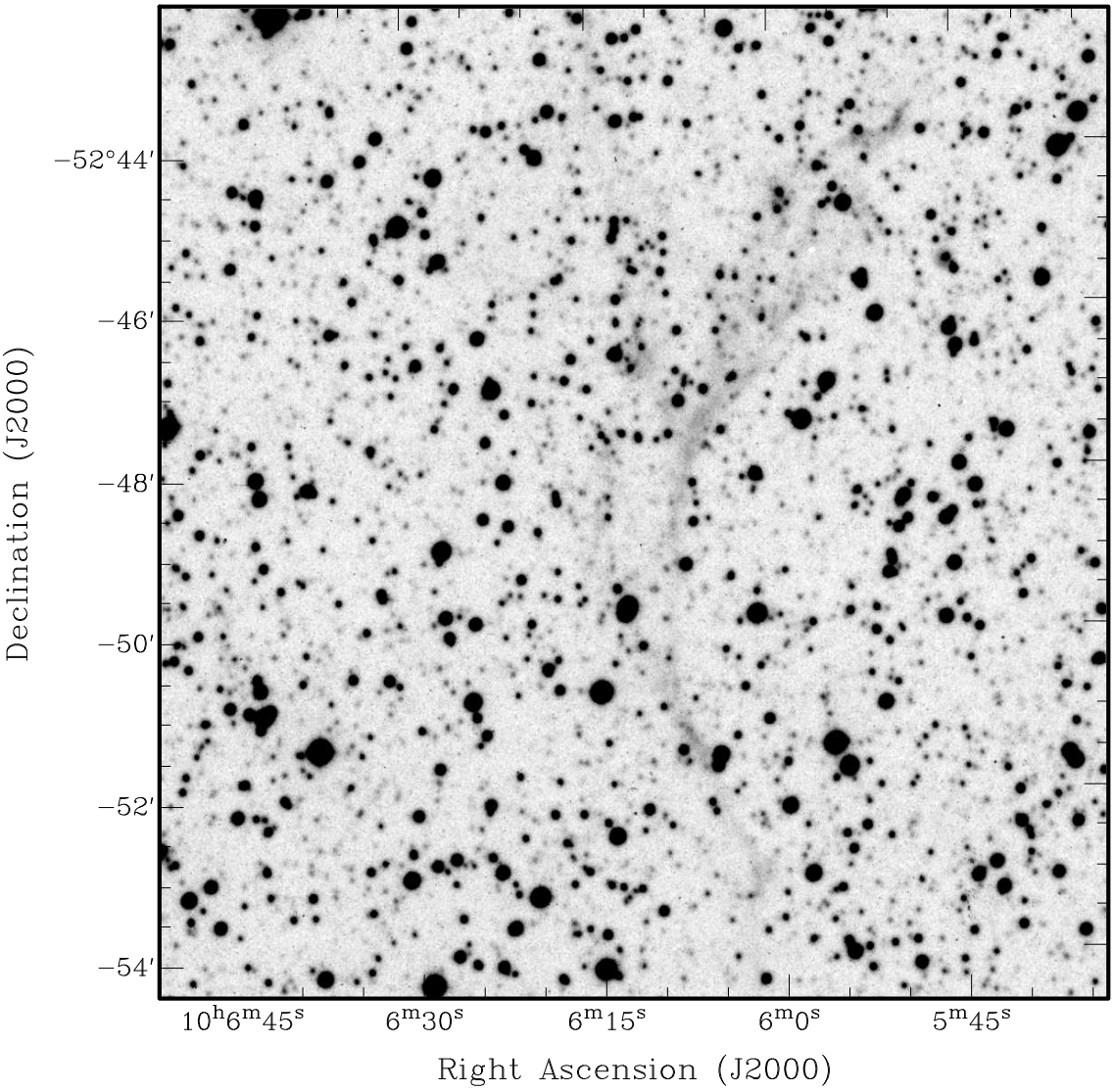

Figure 4.4: Hα image of the brightest filament in G279.0+1.1

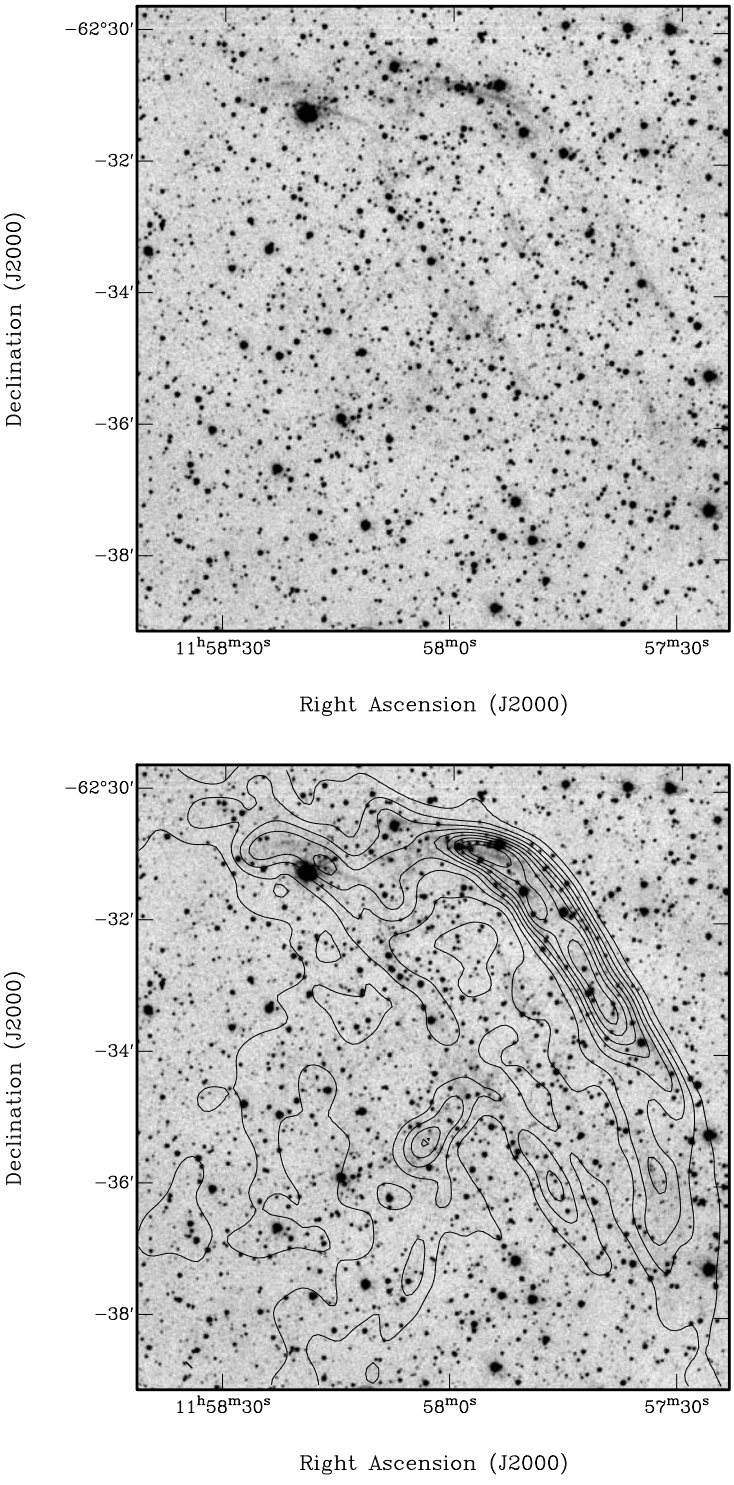

Figure 4.5: a) Hα image of G296.8-0.3 b) Hα image overlaid with ATCA radio image. Contours (mJy/beam) = 5,10,15,20,25,30,35,40,45

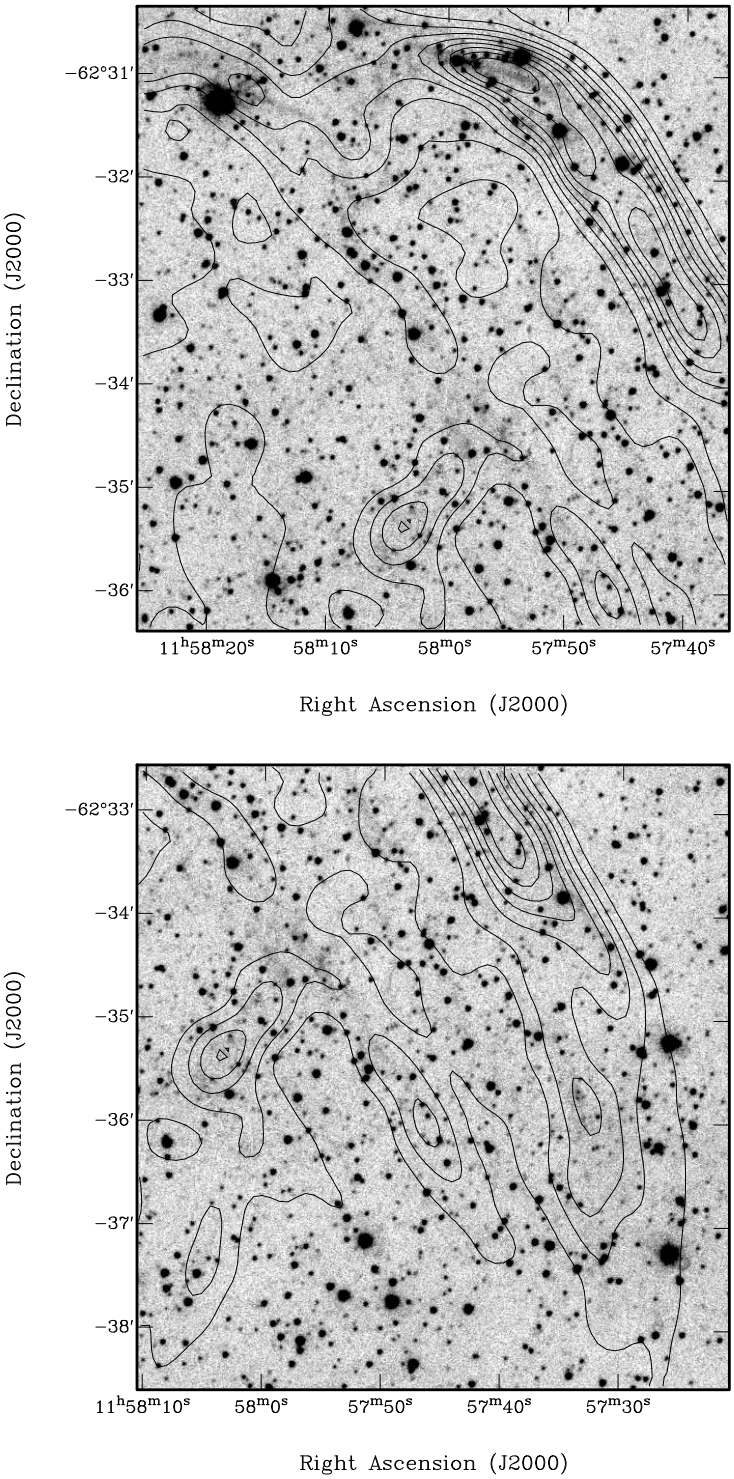

Figure 4.6: Enlarged regions of Fig. 5 overlaid with ATCA radio image. Contours (mJy/beam) = 5,10,15,20,25,30,35,40,45

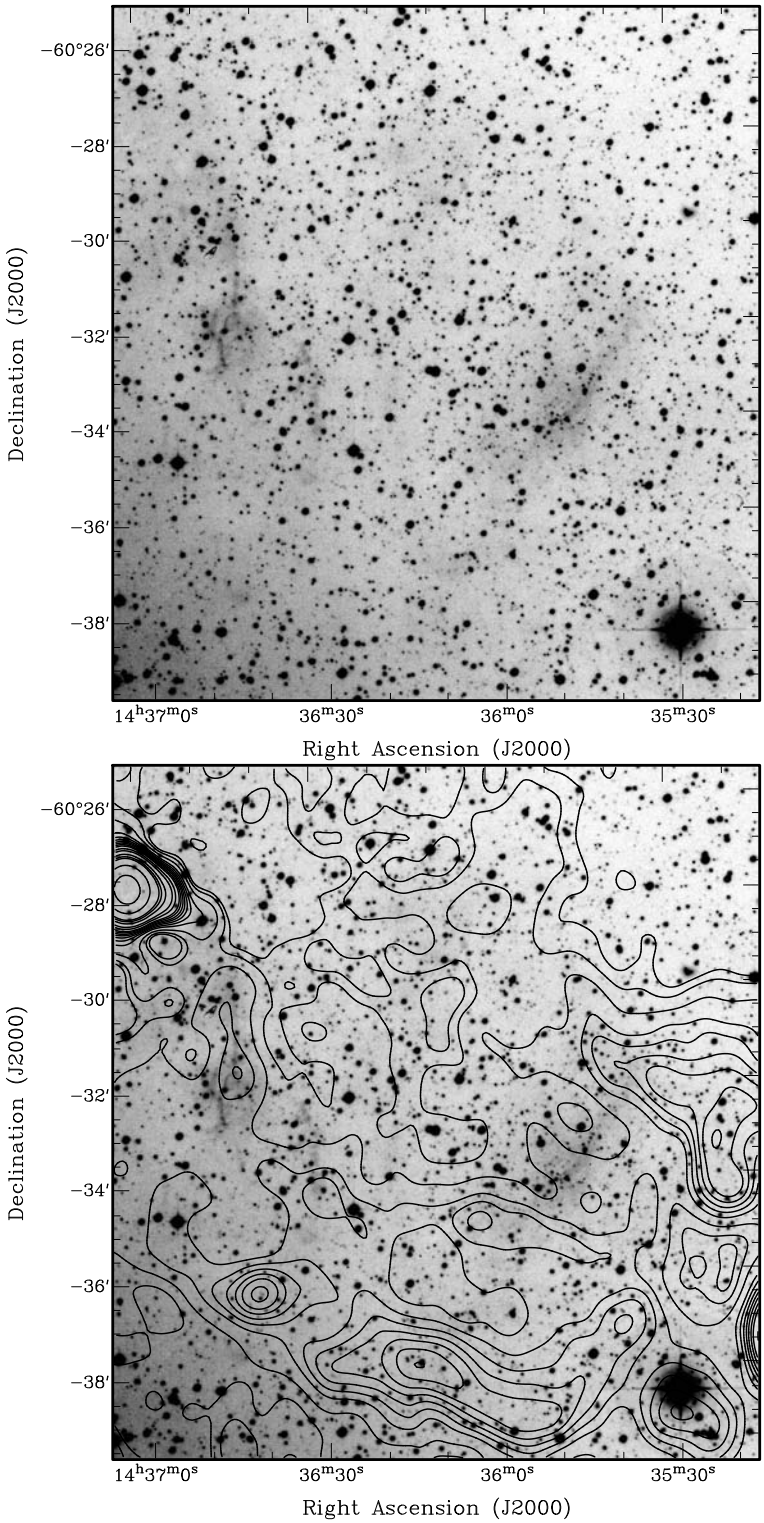

Figure 4.7: a) Hα image of G315.4-0.3 b) Hα image overlaid with MOST radio survey. Contours (mJy/beam) = 2,4,8,14,18,22,26,30,35,40,52, 65,95,120,140,250,450

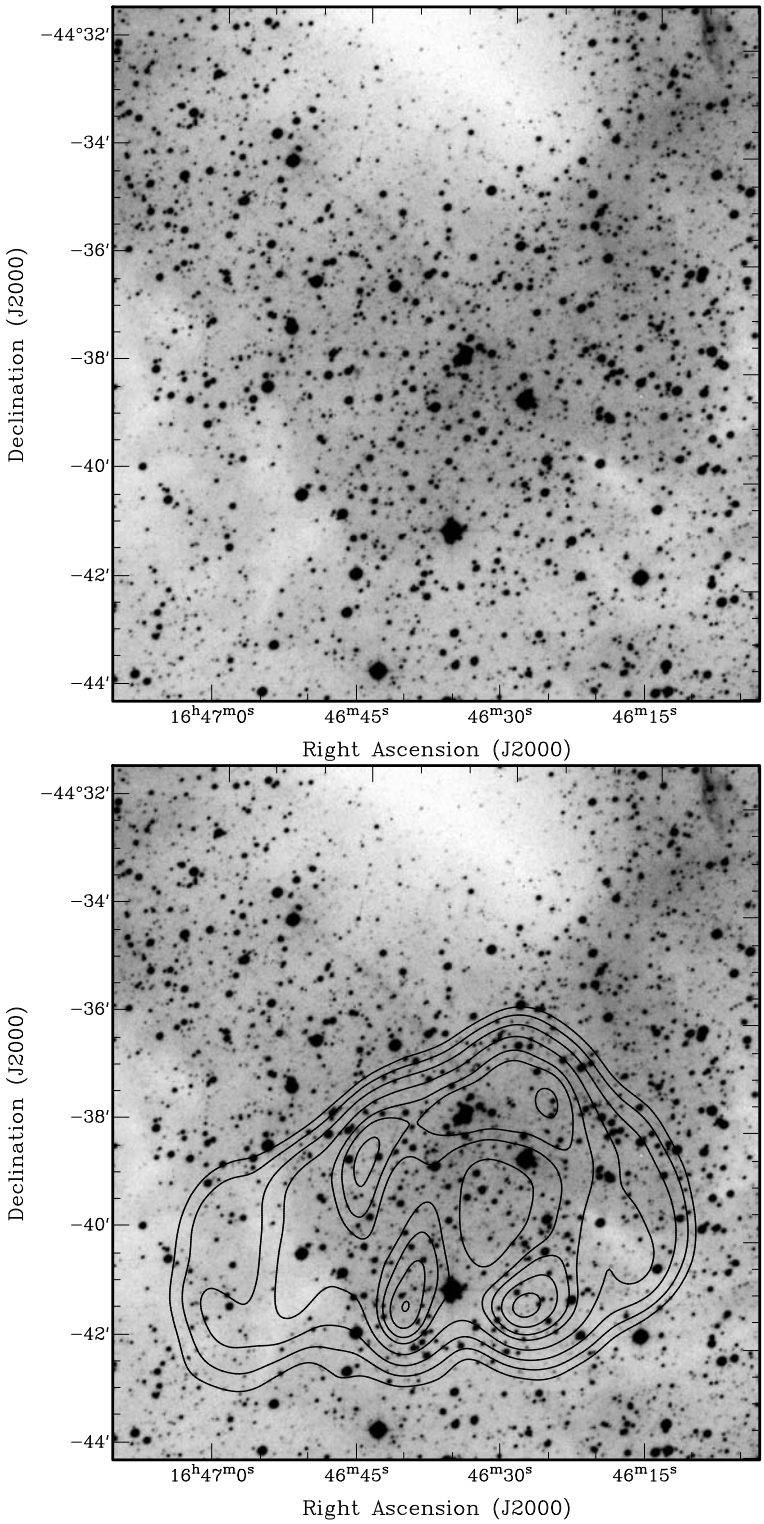

Figure 4.8: a) Hα image of G340.4+0.4 b) Hα image overlaid with MOST radio survey. Contours (mJy/beam) = 10,25,50,90,140,170,210,250,290, 330,360

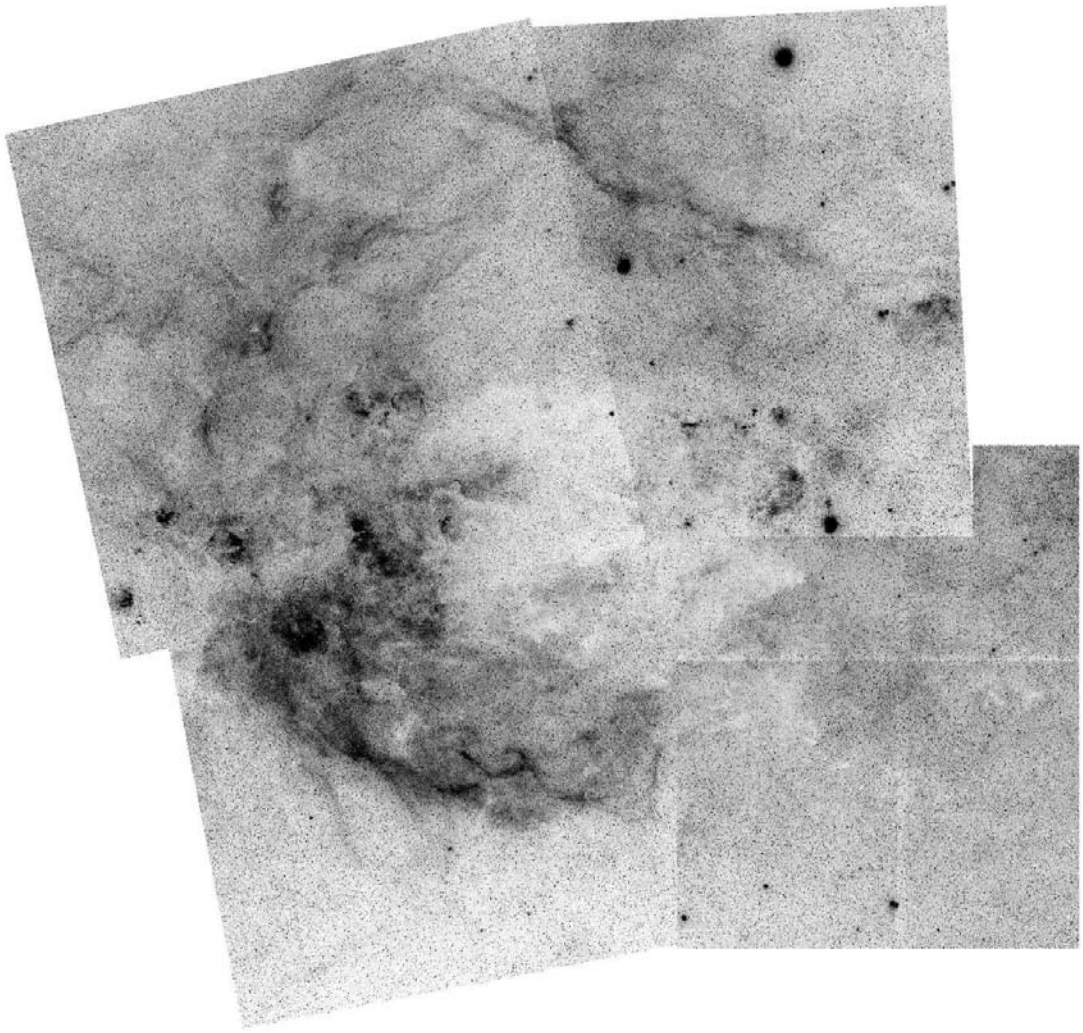

Figure 4.9: The Coalsack Loop. Composite of four Hα images centred on the ESO/SERC Sky Survey fields 95, 96, 131 and 132. Note the presence of the Southern Cross in the upper-right (north-west) portion of the image.

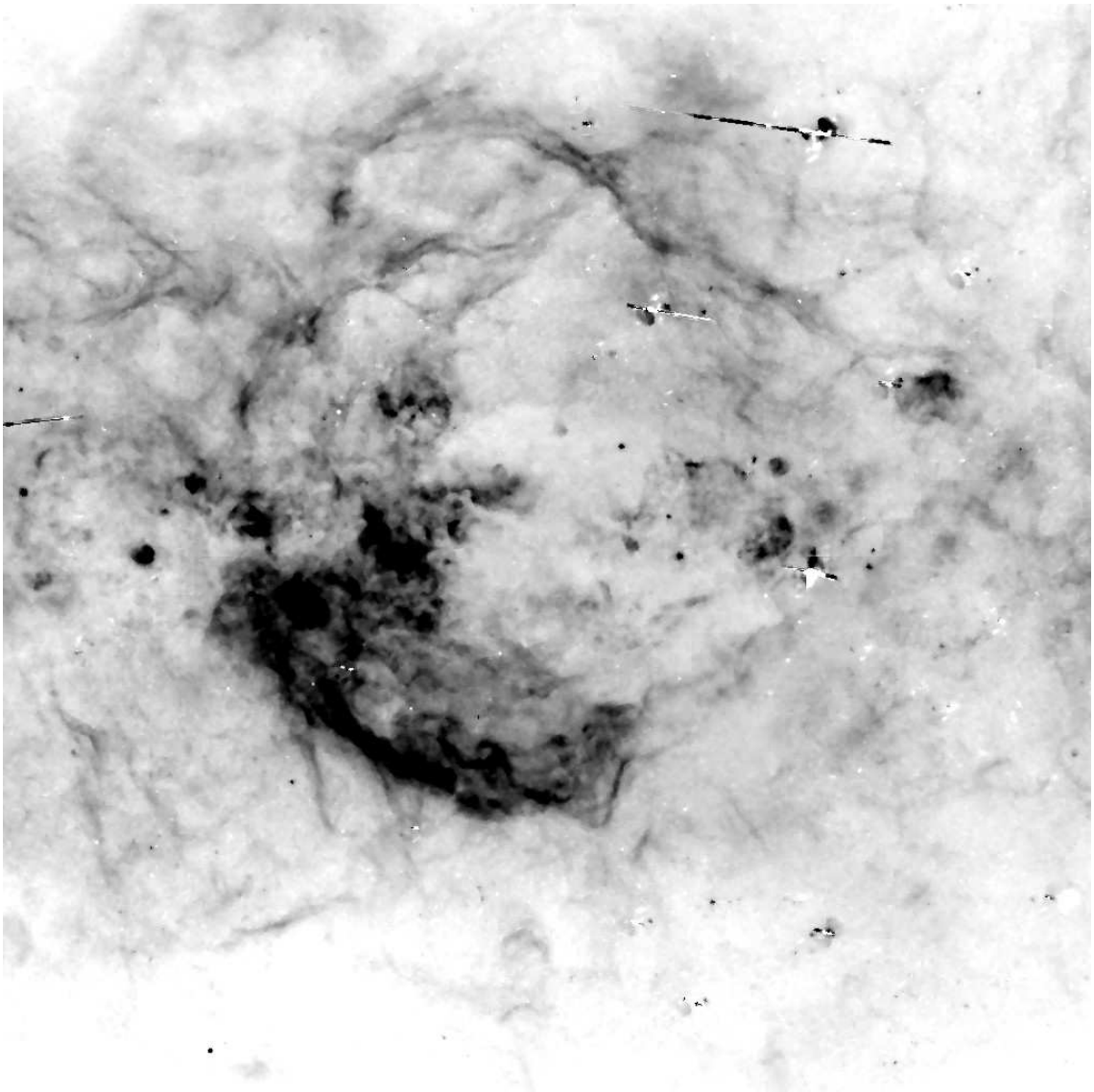

Figure 4.10: Hα image of the Coalsack Loop as seen by the Southern H-Alpha Sky Survey Atlas (SHASSA) survey (details of image and survey in text).

Chapter 5

Conclusions

5.1 Conclusions

In chapter 2, films from the AAO/UKST Hα Survey were used to discover four new large filamentary shell structures, and new optical emission in two known SNR candidates. The combination of Techpan film and an Hα filter allowed the detection of filamentary structure much fainter than in previous photographic surveys, and with improved spatial resolution. Comparison with radio surveys and star catalogues has made it possible to suggest associations with known objects and suggest a powering source for some of these structures. However more detailed observations of individual objects would be needed before their nature can be clearly established.

In chapter 3, we used optical spectroscopy to show that the emission nebula RCW 114 has line ratios consistent with those we would expect to see in an evolved supernova remnant. Weak radio emission was also seen that very closely matched the structure seen optically. The spatial variation of the line ratios [S II]/Hα and [N II]/Hα also show that the expanding shock is interacting more strongly with the surrounding interstellar medium to the south-east, or away from the Galactic plane. A comparison with other large angular diameter SNRs shows that it is the closest and has a small physical size. We suggest that this may be indicative of a weak initial explosion, or it is expanding into a dense medium which has diminished the shock's intensity and resulted in weaker radio emission.

In chapter 4, films from the AAO/UKST Hα Survey were used to look

for optical emission associated with known radio SNRs. 86 SNRs were searched resulting in likely detections of 8 SNRs and possible detections of 4 others. Distance estimates for these objects show that we were able to detect SNR beyond 5 kpc and possibly as far as 10 kpc. In these objects, along with known optical SNRs, the correspondence of the optical emission with radio emission varies from extremely good to poor. We also have discovered a large filamentary structure of 10° in diameter, the Coalsack Loop, which most likely is situated on the far side of the Coalsack Nebula and energised by the Centaurus OB1 association

The work done in this thesis has shown that the nature of filamentary optical emission within our Galaxy is still very poorly understood. The AAO/UKST Hα Survey has resulted in the discovery of many new large size objects, including probable SNRs and Wolf-Rayet shells. It has also added greatly to our knowledge of smaller filamentary objects, especially planetary nebulae. These objects will be especially useful for establishing distances and ages of a larger sample than has been previously possible. This is essential for testing models of their formation and evolution. This will also allow a detailed comparison to be made with the nature of objects in other galaxies, particularly the Magellanic Clouds where their distance is well established.

It has also been seen that to identify the nature of filamentary objects, it is essential to make use of data available in multiple wavelength bands. Each one of these, optical, radio, X-ray and infrared, provides a picture of different shock/ionisation conditions. They also allow for differing parameters of the objects to be measured. In the last few years this has been shown by X-ray observations of SNRs obtained with the Chandra telescope.

Bibliography

L. H. Aller, editor. *Physics of Thermal Gaseous Nebulae*, September 1984.

P. E. Angerhofer, R. G. Strom, T. Velusamy, and M. R. Kundu. A Multifrequency Study of CTB:80 with the Westerbork Synthesis Radio Telescope. A&A, 94: 313, February 1981.

B. Aschenbach. X-ray emission from supernova remnants observed with ROSAT. *Advances in Space Research*, 13:45, December 1993. doi: 10.1016/0273-1177(93)90096-T.

W. Baade. Nova Ophiuchi of 1604 as a Supernova. ApJ, 97:119, March 1943.

W. Baade and R. Minkowski. Identification of the Radio Sources in Cassiopeia, Cygnus a, and Puppis a. ApJ, 119:206, January 1954.

D. K. Bedford, K. H. Elliott, B. Ramsey, and J. Meaburn. Some properties of the filamentary nebula at 1723 - 46. MNRAS, 210:693, October 1984.

W. P. Blair and R. P. Kirshner. Optical spectrum of the unusual supernova remnant G109.1-1.0. Nature, 291:132, May 1981.

W. P. Blair, D. L. Sawyer, R. P. Kirshner, T. R. Gull, and R. A. R. Parker. The discovery of optical emission from the SNR G126.2 + 1.6. ApJ, 242:592, December 1980. doi: 10.1086/158494.

W. P. Blair, R. Sankrit, and J. C. Raymond. Hubble Space Telescope Imaging of the Primary Shock Front in the Cygnus Loop Supernova Remnant. AJ, 129: 2268, May 2005. doi: 10.1086/429381.

D. C.-J. Bock, M. I. Large, and E. M. Sadler. SUMSS: A Wide-Field Radio Imaging Survey of the Southern Sky. I. Science Goals, Survey Design, and Instrumentation. AJ, 117:1578, March 1999. doi: 10.1086/300786.

S. R. Bonsignori-Facondi and P. Tomasi. Evidence for six new low surface brightness supernova remnants. A&A, 77:93, August 1979.

J. Brand and L. Blitz. The Velocity Field of the Outer Galaxy. A&A, 275:67, August 1993.

J. Brand, L. Blitz, and J. G. A. Wouterloot. The velocity field of the outer Galaxy in the Southern Hemisphere. I - Catalogue of nebulous objects. A&AS, 65:537, September 1986.

J. Brand, L. Blitz, J. G. A. Wouterloot, and F. J. Kerr. The velocity field of the outer Galaxy in the Southern Hemisphere. II - CO observations of galactic nebulae. A&AS, 68:1, February 1987.

A. Broadbent, J. L. Osborne, and C. G. T. Haslam. A technique for separating the galactic thermal radio emission from the non-thermal component by means of the associated infrared emission. MNRAS, 237:381, March 1989.

J.-U. Busser, R. Egger, and B. Aschenbach. G299.2-2.9: a new galactic supernova remnant. A&A, 310:L1, June 1996.

M. Buxton, M. Bessell, and B. Watson. The MSSSO wide field CCD H-alpha imaging survey. *Publications of the Astronomical Society of Australia*, 15:24, April 1998.

C. E. Cappa de Nicolau, V. S. Niemela, G. M. Dubner, and E. M. Arnal. The H I bubble around the Wolf-Rayet star HD 156385 and its environs. AJ, 96: 1671, November 1988. doi: 10.1086/114918.

G. L. Case and D. Bhattacharya. A New Sigma -D Relation and Its Application to the Galactic Supernova Remnant Distribution. ApJ, 504:761, September 1998. doi: 10.1086/306089.

J. L. Caswell and D. H. Clark. Observations of radio sources formerly considered as possible supernova remnants. *Australian Journal of Physics Astrophysical Supplement*, page 57, September 1975.

J. L. Caswell, D. K. Milne, and K. J. Wellington. High-resolution radio observations of five supernova remnants. MNRAS, 195:89, April 1981.

J. L. Caswell, R. F. Haynes, D. K. Milne, and K. J. Wellington. Radio maps revealing shell structures in five supernova remnants. MNRAS, 203:595, May 1983.

A. N. Cha, K. R. Sembach, and A. C. Danks. The Distance to the VELA Supernova Remnant. ApJ, 515:L25, April 1999. doi: 10.1086/311968.

R. A. Chevalier. The interaction of supernovae with the interstellar medium. ARA&A, 15:175, 1977. doi: 10.1146/annurev.aa.15.090177.001135.

R. A. Chevalier and J. C. Raymond. Optical emission from a fast shock wave - The remnants of Tycho's supernova and SN 1006. ApJ, 225:L27, October 1978. doi: 10.1086/182785.

D. H. Clark, J. L. Caswell, and A. J. Green. New Galactic Supernova Remnants. Nature, 246:28, November 1973.

D. H. Clark, A. J. Green, and J. L. Caswell. Improved 408 MHz observations of some galactic supernova remnants. *Australian Journal of Physics Astrophysical Supplement*, page 75, September 1975.

F. R. Colomb and G. M. Dubner. Neutral hydrogen associated with southern supernova remnants. I - 'G 261.9, +5.5'. A&A, 82:244, February 1980.

L. E. Cram, A. J. Green, and D. C.-J. Bock. Relationship between Galactic radio continuum and H-alpha emission. *Publications of the Astronomical Society of Australia*, 15:64, April 1998.

I. J. Danziger and M. Dennefeld. Spectroscopy of supernova remnants. A&A, 36: 149, November 1974.

I. J. Danziger and M. Dennefeld. Optical spectra of supernova remnants. PASP, 88:44, February 1976.

M. A. Dopita and R. S. Sutherland. *Astrophysics of the diffuse universe*. Berlin: Springer-Verlag, 1987, 2003.

D. Downes. New Radio Results on Supernova, Remnants. AJ, 76:305, May 1971.

F. D. Drake. On the nature of the composite radio source Cygnus X. In R. N. Bracewell, editor, *IAU Symp. 9: URSI Symp. 1: Paris Symposium on Radio Astronomy*, page 339, 1959.

G. M. Dubner, E. B. Giacani, W. M. Goss, D. A. Moffett, and M. Holdaway. VLA Observations of Nine Galactic Supernova Remnants. AJ, 111:1304, March 1996. doi: 10.1086/117875.

G. M. Dubner, M. Holdaway, W. M. Goss, and I. F. Mirabel. A High-Resolution Radio Study of the W50-SS 433 System and the Surrounding Medium. AJ, 116:1842, October 1998. doi: 10.1086/300537.

A. R. Duncan, R. F. Haynes, R. T. Stewart, and K. L. Jones. The large, highly polarized supernova remnant G 279.0+1.1. MNRAS, 277:319, November 1995a.

A. R. Duncan, R. T. Stewart, R. F. Haynes, and K. L. Jones. A deep radio continuum survey of the southern Galactic plane at 2.4 GHz. MNRAS, 277: 36, November 1995b.

A. R. Duncan, R. T. Stewart, R. F. Haynes, and K. L. Jones. Supernova remnant candidates from the Parkes 2.4-GHz survey. MNRAS, 287:722, June 1997.

K. H. Elliott and D. F. Malin. The optical supernova remnant G290.1-0.8. MNRAS, 186:45P, March 1979.

R. A. Fesen, T. R. Gull, and D. A. Ketelsen. Deep forbidden O III interference filter imagery of the supernova remnants G65.3+5.7, G126.2+1.6, CTA 1, and VRO 42.05.01. ApJS, 51:337, April 1983. doi: 10.1086/190853.

R. A. Fesen, W. P. Blair, and R. P. Kirshner. Optical emission-line properties of evolved galactic supernova remnants. ApJ, 292:29, May 1985. doi: 10.1086/163130.

R. A. Fesen, F. Winkler, Y. Rathore, R. A. Downes, and D. Wallace. Optical Imaging and Spectroscopy of the Galactic Supernova Remnants CTB 1 (G116.9+0.2), G116.5+1.1, and G114.3+0.3. AJ, 113:767, February 1997. doi: 10.1086/118297.

A. V. Filippenko and T. Matheson. Optical, Ultraviolet, and Infrared Observations of SN 1993J. In J.-M. Marcaide and K. W. Weiler, editors, *IAU Colloq. 192: Cosmic Explosions, On the 10th Anniversary of SN1993J*, page 37, 2005.

E. A. Frieman. On Elephant-Trunk Structures in the Region of O Associations. ApJ, 120:18, July 1954.

B. M. Gaensler, R. N. Manchester, and A. J. Green. Radio continuum and HI observations of the supernova remnant G296.8-00.3. MNRAS, 296:813, June 1998.

J. E. Gaustad, P. R. McCullough, W. Rosing, and D. Van Buren. A Robotic Wide-Angle Hα Survey of the Southern Sky. PASP, 113:1326, November 2001.

R. E. Gooch. Grasping the wispy tendrils. *Publications of the Astronomical Society of Australia*, 14:106, April 1997.

W. M. Goss, P. A. Shaver, W. J. Zealey, P. Murdin, and D. H. Clark. Optical identification and spectrum of the supernova remnant G292.0+1.8. MNRAS, 188:357, August 1979.

D. A. Green. Limitations imposed on statistical studies of Galactic supernova remnants by observational selection effects. PASP, 103:209, February 1991.

D. A. Green. Statistical studies of supernova remnants. MNRAS, 209:449, July 1984.

D. A. Green. A catalogue of galactic supernova remnants (2000 august version), 2000. Mullard Radio Astronomy Observatory, Cambridge, United Kingdom (available on the World-Wide-Web at "http://www.mrao.cam.ac.uk/surveys/snrs/").

J. Greiner, R. Egger, and B. Aschenbach. G272.2-3.2: a centrally filled and possibly young SNR discovered by ROSAT. A&A, 286:L35, June 1994.

M. R. Griffith and A. E. Wright. The Parkes-MIT-NRAO (PMN) surveys. I - The 4850 MHz surveys and data reduction. AJ, 105:1666, May 1993. doi: 10.1086/116545.

C. Guillermo Gimenez de Castro and V. S. Niemela. CCD images and long-slit spectroscopy of the ring nebula around theta MUS. MNRAS, 297:1060, July 1998.

S. F. Gull. A numerical model of the structure and evolution of young supernovaremnants. MNRAS, 161:47, 1973.

T. R. Gull, R. P. Kirshner, and R. A. R. Parker. A new optical supernova remnant in Cygnus. ApJ, 215:L69, July 1977.

N. C. Hambly, L. Miller, H. T. MacGillivray, J. T. Herd, and W. A. Cormack. Precision astrometry with SuperCOSMOS. MNRAS, 298:897, August 1998. doi: 10.1046/j.1365-8711.1998.01669.x.

R. Hanbury Brown, H. P. Palmer, and A. R. Thompson. Galactic radio sources of large angular diameter. Nature, 173:945, 1954.

D. E. Harris and J. A. Roberts. Radio Source Measurements at 960 Mc/s. PASP, 72:237, August 1960.

J. N. Heckathorn, F. C. Bruhweiler, and T. R. Gull. A new search for nebulae surrounding Wolf-Rayet stars. ApJ, 252:230, January 1982. doi: 10.1086/159550.

E. R. Hill. Some observations of shell-type galactic radio sources. *Australian Journal of Physics*, 20:297, 1967.

U. Hwang and T. H. Markert. An X-ray study of five supernova remnants in the Carina spiral arm. ApJ, 431:819, August 1994. doi: 10.1086/174532.

N. J. Irvine and C. E. Irvine. A new optical supernova remnant in Centaurus. ApJ, 192:L111, September 1974.

J. B. Kaler. Planetary nebulae and their central stars. ARA&A, 23:89, 1985. doi: 10.1146/annurev.aa.23.090185.000513.

M. J. Kesteven and J. L. Caswell. Barrel-shaped supernova remnants. A&A, 183: 118, September 1987.

R. P. Kirshner and P. F. J. Winkler. Discovery of Optical Emission from the SNR G290.1-0.8. ApJ, 227:853, February 1979. doi: 10.1086/156794.

C. R. Kitchin. *Stars, nebulae and the interstellar medium. Observational physics and astrophysics*. Bristol: Hilger, 1987, 1987.

B. Koralesky, D. A. Frail, W. M. Goss, M. J. Claussen, and A. J. Green. Shock-excited Maser Emission from Supernova Remnants: G32.8-0.1, G337.8-0.1, G346.6-0.2, and the HB 3/W3 Complex. AJ, 116:1323, September 1998. doi: 10.1086/300508.

M. I. Large and A. E. Vaughan. Pulsars-A new pulsar-supernova association. Nature, 236:117, April 1972.

K. S. Long and W. P. Blair. The identification of Balmer-dominated filaments in RCW 86. ApJ, 358:L13, July 1990. doi: 10.1086/185768.

A. J. Longmore, D. H. Clark, and P. Murdin. A new optical supernova remnant in Crux. MNRAS, 181:541, December 1977.

T. A. Lozinskaya. *Supernovae and stellar wind in the interstellar medium*. New York: American Institute of Physics, 1992, 1992.

T. A. Lozinskaya, T. G. Sitnik, and V. V. Pravdikova. Optical emission of the supernova remnant G73.9+0.9. *Astronomy Reports*, 37:240, May 1993.

A. P. Marston. A Survey of Nebulae around Galactic Wolf-Rayet Stars in the Southern Sky. III. Survey Completion and Conclusions. ApJ, 475:188, January 1997. doi: 10.1086/303534.

A. P. Marston, Y.-H. Chu, and G. Garcia-Segura. A survey of nebulae around Galactic Wolf-Rayet stars in the southern sky, 1. ApJS, 93:229, July 1994a. doi: 10.1086/192053.

A. P. Marston, D. R. Yocum, G. Garcia-Segura, and Y.-H. Chu. A survey of nebulae around galactic wolf-rayet stars in the southern sky, 2. ApJS, 95:151, November 1994b. doi: 10.1086/192097.

F. Mavromatakis, J. Papamastorakis, J. Ventura, W. Becker, E. V. Paleologou, and D. Schaudel. The supernova remnants G 67.7+1.8, G 31.5-0.6 and G 49.2-0.7. A&A, 370:265, April 2001. doi: 10.1051/0004-6361:20010137.

N. M. McClure-Griffiths, J. M. Dickey, B. M. Gaensler, and A. J. Green. H I Shells behind the Coalsack. ApJ, 562:424, November 2001. doi: 10.1086/323859.

J. Meaburn and P. Rovithis. A New Large Supernova Remnant in the Southern Sky? Ap&SS, 46:L7, February 1977.

J. Meaburn, C. Goudis, N. Solomos, and V. Laspias. Optical and far-infrared observations of the galactic filamentary nebula at 1723 - 46. A&A, 252:291, December 1991.

G. J. Miller and Y.-H. Chu. A new survey of nebulae around Galactic Wolf-Rayet stars in the northern sky. ApJS, 85:137, March 1993. doi: 10.1086/191757.

L. Miller, W. Cormack, M. Paterson, S. Beard, and L. Lawrence. Supercosmos. In H. T. MacGillivray and E. B. Thomson, editors, *ASSL Vol. 174: Digitised Optical Sky Surveys*, page 133, 1992.

B. Y. Mills, O. B. Slee, and E. R. Hill. A Catalogue of Radio Sources between Declinations -20° and -50°. *Australian Journal of Physics*, 13:676, 1960.

D. K. Milne. Nonthermal galactic radio sources. *Australian Journal of Physics*, 23:425, June 1970.

R. Minkowski. Cygnus Loop and Some Related Nebulosities. In J. M. Burgers and R. N. Thomas, editors, *IAU Symp. 8: Cosmical Gas Dynamics*, page 1048, 1958.

R. Minkowski. Optical investigations of radio sources (Introductory Lecture). In H. C. van de Hulst, editor, *IAU Symp. 4: Radio astronomy*, page 107, 1957.

W. W. Morgan, B. Strömgren, and H. M. Johnson. A Description of Certain Galactic Nebulosities. ApJ, 121:611, May 1955.

Q. Parker and F. Watson. A Flair for Wide-Field Spectroscopy. In S. J. Maddox and A. Aragon-Salamanca, editors, *Wide Field Spectroscopy and the Distant Universe*, page 33, 1995.

Q. A. Parker and J. Bland-Hawthorn. Technical aspects of the new AAO/UKST H-alpha interference filter. *Publications of the Astronomical Society of Australia*, 15:33, April 1998.

Q. A. Parker and D. Malin. The introduction of Tech Pan film at the UK Schmidt Telescope. *Publications of the Astronomical Society of Australia*, 16:288, December 1999.

Q. A. Parker and S. Phillipps. Background and first results from the new AAO/UKST H-alpha Survey. *Publications of the Astronomical Society of Australia*, 15:28, April 1998.

Q. A. Parker, S. Phillipps, and D. H. Morgan. The AAO/UKST H-alpha Survey. In A. R. Taylor, T. L. Landecker, and G. Joncas, editors, *ASP Conf. Ser. 168: New Perspectives on the Interstellar Medium*, page 126, 1999.

W. Reich, E. Fürst, P. Reich, and N. Junkes. New Supernova Remnants from Deep Radio Continuum Surveys. In R. S. Roger and T. L. Landecker, editors, *IAU Colloq. 101: Supernova Remnants and the Interstellar Medium*, page 293, 1988.

W. Reich, E. Fuerst, P. Reich, and K. Reif. A radio continuum survey of the Galactic Plane at 11 CM wavelength. II - The area L = 358-76 deg, B = -5 to 5 deg. III. A&AS, 85:633, October 1990.

S. P. Reynolds. *Supernova remnants*, page 439. Galactic and Extragalactic Radio Astronomy, 1988.

J. Rho, R. Petre, E. M. Schlegel, and J. J. Hester. An X-ray and optical study of the supernova remnant W44. ApJ, 430:757, August 1994. doi: 10.1086/174446.

M. Rosado, P. Ambrocio-Cruz, E. Le Coarer, and M. Marcelin. Kinematics of the galactic supernova remnants RCW 86, MSH 15-56 and MSH 11-61A. A&A, 315:243, November 1996.

S. D. Ryder, C. E. Murrowood, and R. A. Stathakis. A postmortem investigation of the Type IIb supernova 2001ig. *preprint (astroph/0603336)*, 2006.

F. Sabbadin. Spectroscopic observations of filamentary nebulae in the Cygnus X region. A&A, 51:159, August 1976.

O. Schwentker. Evidence for a low-luminosity X-ray pulsar associated with a supernova remnant. A&A, 286:L47, June 1994.

K. J. Seidensticker and T. Schmidt-Kaler. The distance and structure of the Coalsack. II - Analysis. A&A, 225:192, November 1989.

F. D. Seward, T. M. Dame, R. A. Fesen, and B. Aschenbach. A ROSAT-detected, New Galactic Supernova Remnant in Sagittarius, G13.3-1.3. ApJ, 449:681, August 1995. doi: 10.1086/176089.

R. C. Smith. The discovery of Balmer-Filaments Encircling SNR RCW 86. AJ, 114:2664, December 1997. doi: 10.1086/118676.

K. Z. Stanek, T. Matheson, P. M. Garnavich, P. Martini, P. Berlind, N. Caldwell, P. Challis, W. R. Brown, R. Schild, K. Krisciunas, M. L. Calkins, J. C. Lee, N. Hathi, R. A. Jansen, R. Windhorst, L. Echevarria, D. J. Eisenstein, B. Pindor, E. W. Olszewski, P. Harding, S. T. Holland, and D. Bersier. Spectroscopic Discovery of the Supernova 2003dh Associated with GRB 030329. ApJ, 591: L17, July 2003. doi: 10.1086/376976.

S. van den Bergh. An Optical Search for Possible Supernova Remnants. *Zeitschrift fur Astrophysik*, 51:15, 1960.

S. van den Bergh. The optical remnant of the Lupus SN of 1006. ApJ, 208:L17, August 1976. doi: 10.1086/182222.

S. van den Bergh. The Optical Remnant of W50 = SS433. ApJ, 236:L23, February 1980. doi: 10.1086/183190.

S. van den Bergh. Optical identification of the peculiar supernova remnant G 326.3-1.8. ApJ, 227:497, January 1979. doi: 10.1086/156757.

S. van den Bergh. Observations of the Optical Remnant of SN 1181 = 3c 58. ApJ, 220:L9, February 1978. doi: 10.1086/182626.

S. van den Bergh and W. Herbst. Catalogue of southern stars embedded in nebulosity. AJ, 80:208, March 1975.

S. van den Bergh, A. P. Marscher, and Y. Terzian. An Optical Atlas of Galactic Supernova Remnants. ApJS, 26:19, August 1973.

A. Walker and W. J. Zealey. Searching for supernova remnants. *Publications of the Astronomical Society of Australia*, 15:79, April 1998.

A. J. Walker, W. J. Zealey, and Q. A. Parker. Filamentary Shell Structures from the AAO/UKST Hα Survey. *Publications of the Astronomical Society of Australia*, 18:259, 2001. doi: 10.1071/AS01063.

K. W. Weiler and R. A. Sramek. Supernovae and supernova remnants. ARA&A, 26:295, 1988. doi: 10.1146/annurev.aa.26.090188.001455.

J. B. Z. Whiteoak. A new composite supernova remnant of low surface brightness - G322.5 - 0.1. MNRAS, 256:121, May 1992.

J. B. Z. Whiteoak and A. J. Green. The MOST supernova remnant catalogue (MSC). A&AS, 118:329, August 1996.

B. Woermann and J. L. Jonas. G279.0 + 1.1 - A new large-diameter galactic supernova remnant. MNRAS, 234:971, October 1988.

L. Woltjer. Supernova Remnants. ARA&A, 10:129, 1972. doi: 10.1146/annurev.aa.10.090172.001021.

K. M. Xilouris, J. Papamastorakis, E. V. Paleologou, Y. Andredakis, and G. Haerendel. Detection of optical emission in the area of G127.1+0.5. A&A, 270:393, March 1993.

W. J. Zealey, K. H. Elliott, and D. F. Malin. New optical observations of galactic supernova remnants. A&AS, 38:39, October 1979.

W. J. Zealey, M. A. Dopita, and D. F. Malin. The interaction between the relativistic jets of SS433 and the interstellar medium. MNRAS, 192:731, September 1980.